Supporting Information

Non-covalent and Dynamic Covalent Chemistry Strategies for Driving Thermoresponsive Phase Transition with Multi-stimuli and Controlled Encapsulation/Release

Imran Khan,[a,b] Junling Wang,[a] Hanxun Zou,[a,b,*] Hebo Ye,[a] Daijun Zha,[a] Yi Zhang,[c,*]

and Lei You,[a,b,*]

a. State Key Laboratory of Structural Chemistry, Fujian Institute of Research on the Structure of Matter, Chinese Academy of Sciences, Fuzhou, Fujian 350002, China.

b. University of Chinese Academy of Sciences, Beijing 100049, China.

c. School of Materials Science and Energy Engineering, Foshan University, Foshan, Guangdong 528000, China.

Email: lyou@fjirsm.ac.cn, imzhy@fosu.edu.cn, zouhanxun@fjirsm.ac.cn

TABLE OF CONTENTS

1. Experimental Section

Synthesis and characterization of monomers

Scheme S1. The Synthesis of Monomer **CN**.

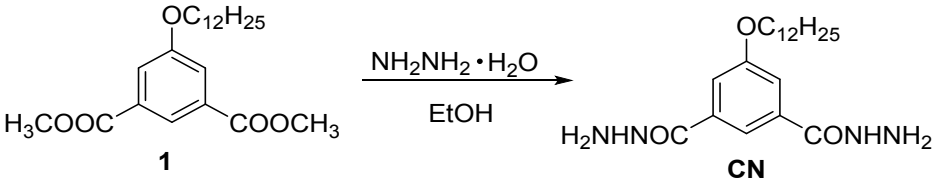

Synthesis of monomer **CN**.[S1,S2] To a solution of compound **1**[S1] (0.50 g, 1.32 mmol) in ethanol (20 mL), was added hydrazine monohydrate (1.25 mL). The solution was refluxed for 14 h and the mixture was concentrated to a small volume after cooling down to room temperature. The precipitate was collected and then washed with water for three times. The solid was dried under vacuum to afford compound **CN** as a white powder (0.29 g, 58%). ^{1}H NMR (DMSO-d_6): δ 9.78 (s, 2H), 7.85 (s, 1H), 7.45 (s, 2H), 4.51 (br, 4H), 4.03 (t, J = 6.4 Hz, 2H), 1.76-1.69 (m, 2H), 1.44-1.38 (m, 2H), 1.34-1.24 (m, 16H), 0.86 (t, J = 6.4 Hz, 3H).^{13}C NMR (DMSO-d_6): δ 165.6, 158.9, 135.2, 118.8, 115.7, 68.4, 31.8, 29.5, 29.2, 29.1, 25.9, 22.6, 14.4. ESI-HRMS: m/z calculated for $C_{20}H_{35}N_4O_3$ $[M + H]^+$: 379.2709; found: 379.2716.

Scheme S2. The Synthesis of Monomer **PN**.

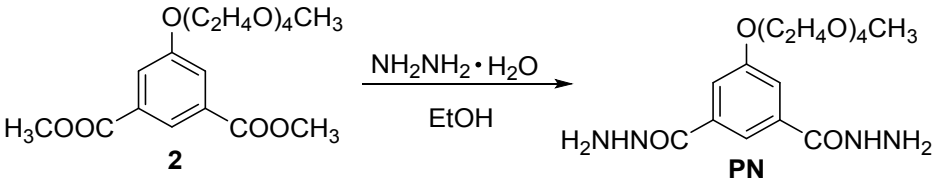

Synthesis of monomer **PN**.[S1,S2] To a solution of compound **2**[S1] (0.50 g, 1.25 mmol) in ethanol (15 mL), was added hydrazine monohydrate (1.0 mL). The solution was refluxed for 14 h, and the mixture was concentrated to a small volume after cooling down to room temperature. The precipitate was collected and then washed with water for three times. The solid was dried under vacuum to afford compound **PN** as a pale yellow solid (0.30 g, 60%). ^{1}H NMR (DMSO-d_6): δ 9.78 (s, 2H), 7.86 (s, 1H), 7.48 (s, 2H), 4.50 (br, 4H), 4.19 (t, J = 4.8 Hz, 2H), 3.78 (t, J = 4.8 Hz, 2H), 3.61-3.59 (m, 2H), 3.55-3.49 (m, 8H), 3.42-3.40 (m, 2H), 3.22 (s, 3H). ^{13}C NMR (DMSO-d_6): δ

165.6, 158.7, 135.3, 119.0, 115.7, 71.7, 70.4, 70.3, 70.2, 70.0, 69.2, 68.0, 58.5. ESI-HRMS: m/z calculated for $C_{17}H_{28}N_4O_7Na$ $[M + Na]^+$: 423.1856; found: 423.1624.

Scheme S3. The Synthesis of Monomer **PO**.

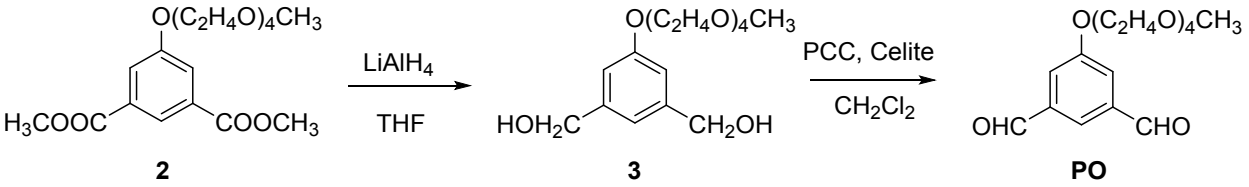

Synthesis of monomer **PO**.[S2,S3] A solution of compound **2**[S1] (0.60 g, 1.5 mmol) in anhydrous THF (10.0 mL) was added dropwise to an ice-cold suspension of $LiAlH_4$ (0.23 g, 6.0 mmol) in THF (10.0 mL). The resulting mixture was refluxed for 3 h, and the completion of the reaction was confirmed by TLC (CH_2Cl_2/MeOH 95:5). The reaction was quenched with water (2.0 mL). The mixture was filtered, and the solvent was removed under vacuum. The residue was extracted with EtOAc and washed with brine. The organic layer was dried overNa_2SO_4 and evaporated. The resulting crude product was used for next step without further purification.

Compound **3** (0.15 g, 0.44 mmol), Celite (0.50 g), and pyridinium chlorochromate (PCC, 0.38 g, 1.77 mmol) were mixed in dichloromethane (20.0 mL). After stirring at room temperature overnight, the reaction mixture was filtered. The filtrate was extracted with EtOAc and washed with brine. The organic layer was dried over Na_2SO_4 and evaporated. The crude product was purified by column chromatography (CH_2Cl_2/MeOH 50:1) to afford compound **PO** as a pale yellow oil (0.13 g, 89%). ^{1}H NMR ($CDCl_3$): δ 10.04 (s, 2H), 7.96 (s, 1H),7.68 (s, 2H), 4.25 (t, J = 4.4 Hz, 2H), 3.91 (t, J = 4.4 Hz, 2H), 3.75-3.73 (m, 2H), 3.69-3.63 (m, 8H), 3.55-3.53 (m, 2H), 3.37 (s, 3H). ^{13}C NMR ($CDCl_3$): δ 190.9, 160.0, 138.2, 124.1, 120.1, 71.8, 70.8, 70.5, 70.5, 70.4, 69.4, 68.2, 58.9. ESI-HRMS: m/z calculated for for $C_{17}H_{24}O_7Na$ $[M + Na]^+$: 363.1420; found: 363.1414.

Scheme S4. The Synthesis of Monomer **CO**.

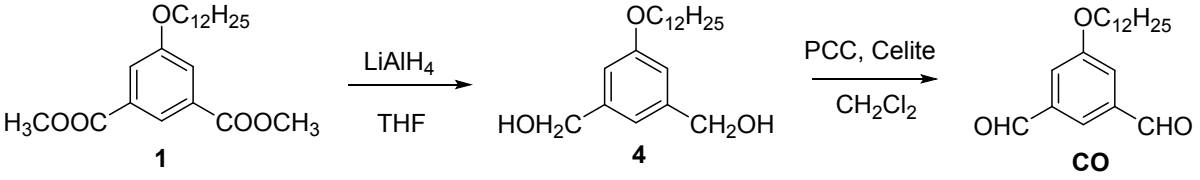

Synthesis of monomer **CO**.[S2,S3] A solution of compound **1**[S1] (1.0 g, 2.64 mmol) in anhydrous THF (15.0 mL) was added dropwise to an ice-cold suspension of $LiAlH_4$ (0.4 g, 10.56 mmol) in THF (15.0 mL). The resulting mixture was refluxed for 3 h, and the completion of the reaction was confirmed by TLC (CH_2Cl_2/MeOH 20:1). The reaction was quenched with water (2.0 mL). The mixture was filtered, and the solvent was removed under vacuum. The residue was extracted with EtOAc and washed with brine. The organic layer was dried (Na_2SO_4) and evaporated. The resulting crude product was used for next step without further purification.

Compound **4** (0.50 g, 1.55 mmol), Celite (1.76 g), and pyridinium chlorochromate (PCC, 1.33 g, 6.20 mmol) were mixed in dichloromethane (50.0 mL). After stirring at room temperature overnight, the reaction mixture was filtered. The filtrate was extracted with EtOAc and washed with brine. The organic layer was dried over Na_2SO_4 and evaporated. The crude product was purified by column chromatography (dichloromethane) to afford compound **CO** as a pale yellow oil (0.40 g, 81%). ^{1}H NMR ($CDCl_3$): δ 10.05 (s, 2H), 7.94 (s, 1H), 7.64 (d, 2H), 4.10 (t, J = 6.8 Hz, 2H), 1.85-1.79 (m, 2H), 1.51-1.44 (m, 2H), 1.38-1.26 (m, 16H), 0.90 (t, J = 6.4 Hz, 3H). ^{13}C NMR ($CDCl_3$): δ 191.0, 160.4, 138.3 , 123.9, 119.9, 68.9, 31.9, 29.7, 29.6 29.3, 29.0, 25.9, 22.7, 14.1. ESI-HRMS: m/z calculated for $C_{20}H_{30}O_3Na$ $[M + Na]^+$: 341.2093; found: 341.2632.

Preparation of dynamic covalent polymers

Synthesis of polymers **POCN** and **COPN**. To a solution of dialdehyde and dihydrazide (the feed ratio was 1:1) in methanol, trifluoroacetic acid (TFA, 0.1 equiv.) was added. The mixture was heated to reflux for 24 h. After cooling down to room temperature, the precipitate was filtered and washed with MeOH thoroughly. After dried under vacuum at room temperature, the pure dynamic covalent polymers containing the acylhydrazone bond was obtained.

Synthesis of polymer **POPN**. To a solution of dialdehyde and dihydrazide (the feed ratio was 1:1) in methanol, trifluoroacetic acid (TFA, 0.1 equiv.) was added. The mixture was heated to reflux for 24 h. The bulk polymer was extracted with 100 ml of refluxing hexane by using a Soxhlet extractor for 24 h. After extraction, the resulting solid was washed with diethyl ether, and the product was dried under vacuum to afford **POPN** as a yellow solid.

^{1}H NMR and ^{13}C NMR spectra

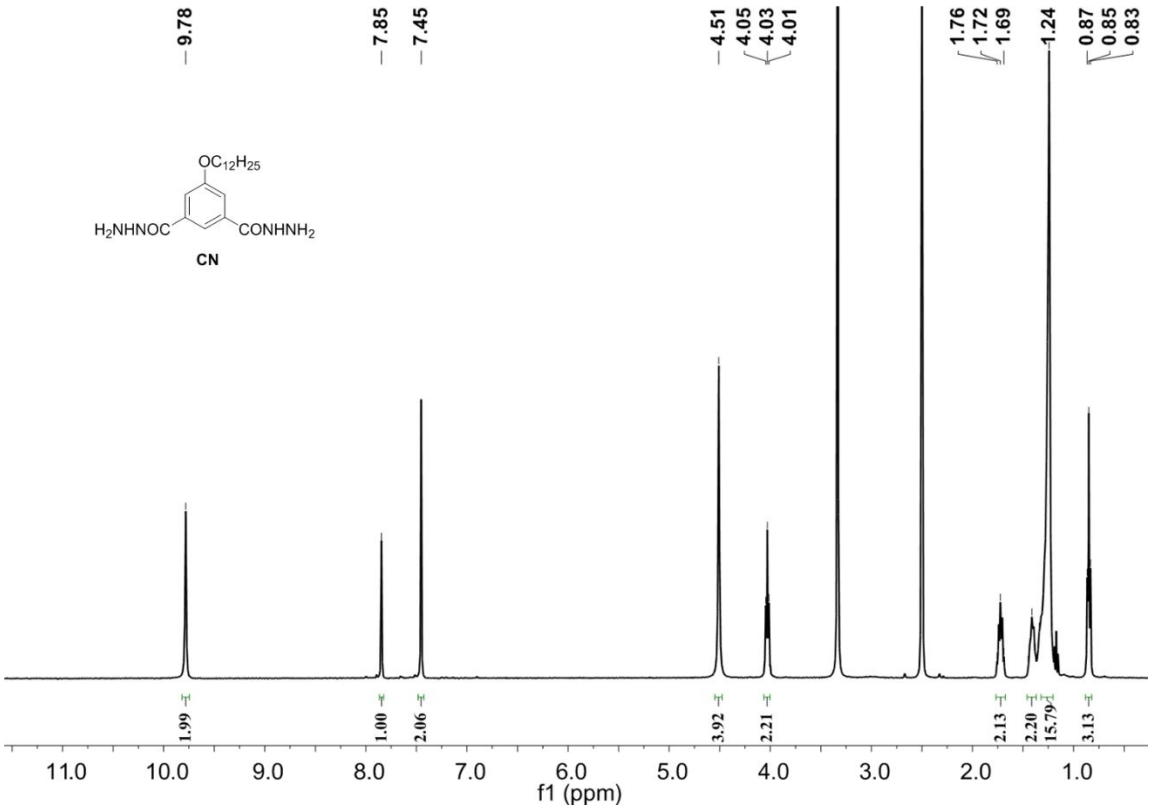

Figure S1. ^{1}H NMR spectrum of monomer **CN** in DMSO-d_6.

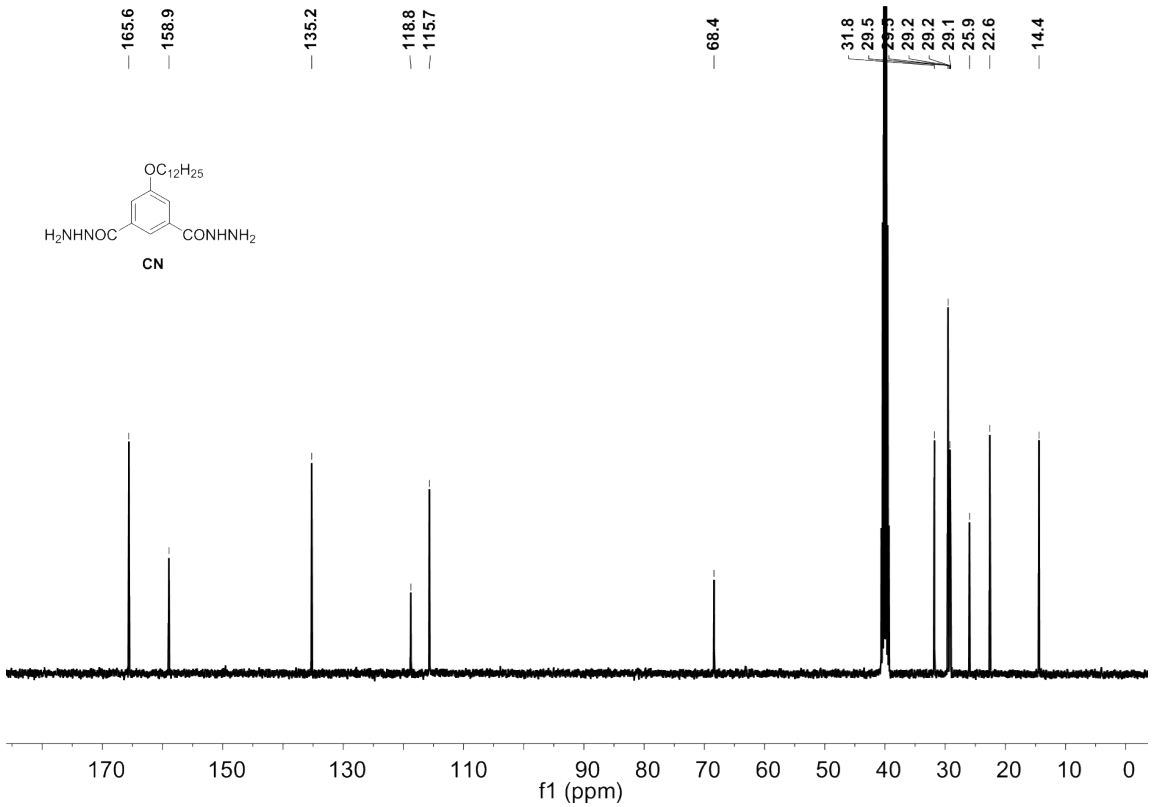

Figure S2. ^{13}C NMR spectrum of monomer **CN** in DMSO-d_6.

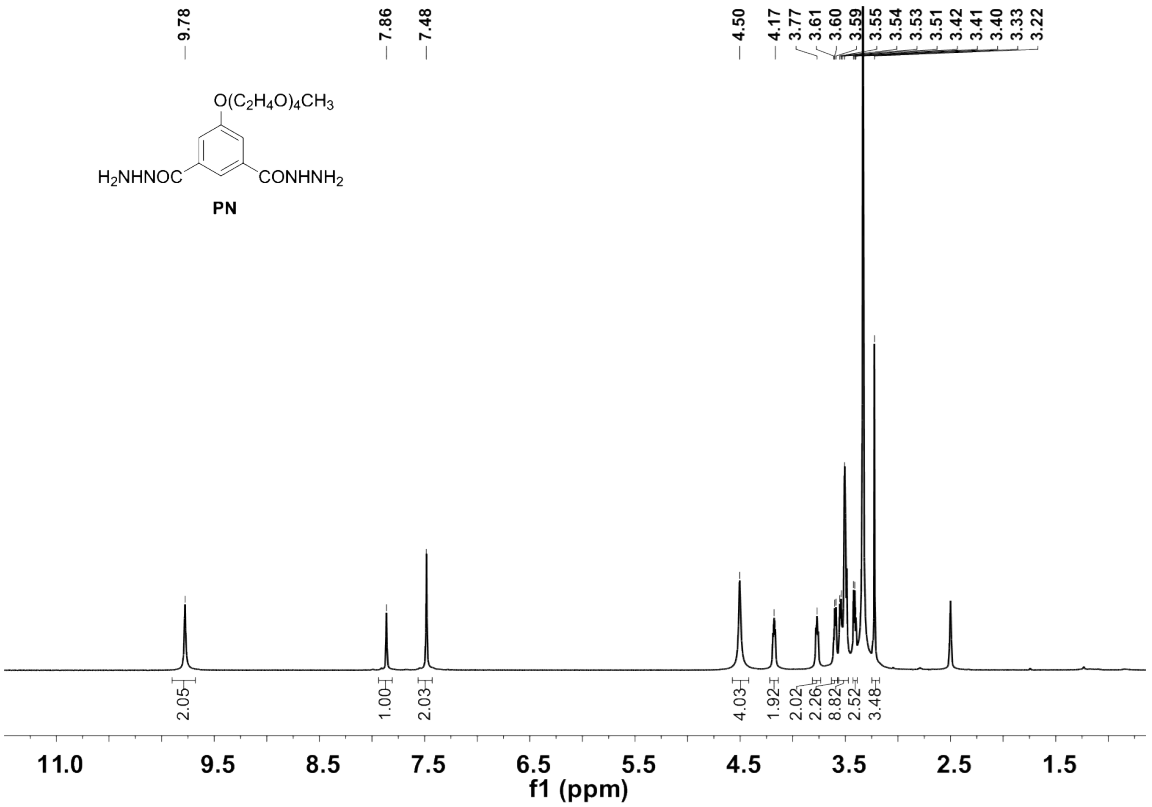

Figure S3. ^{1}H NMR spectrum of monomer **PN** in DMSO-d_6.

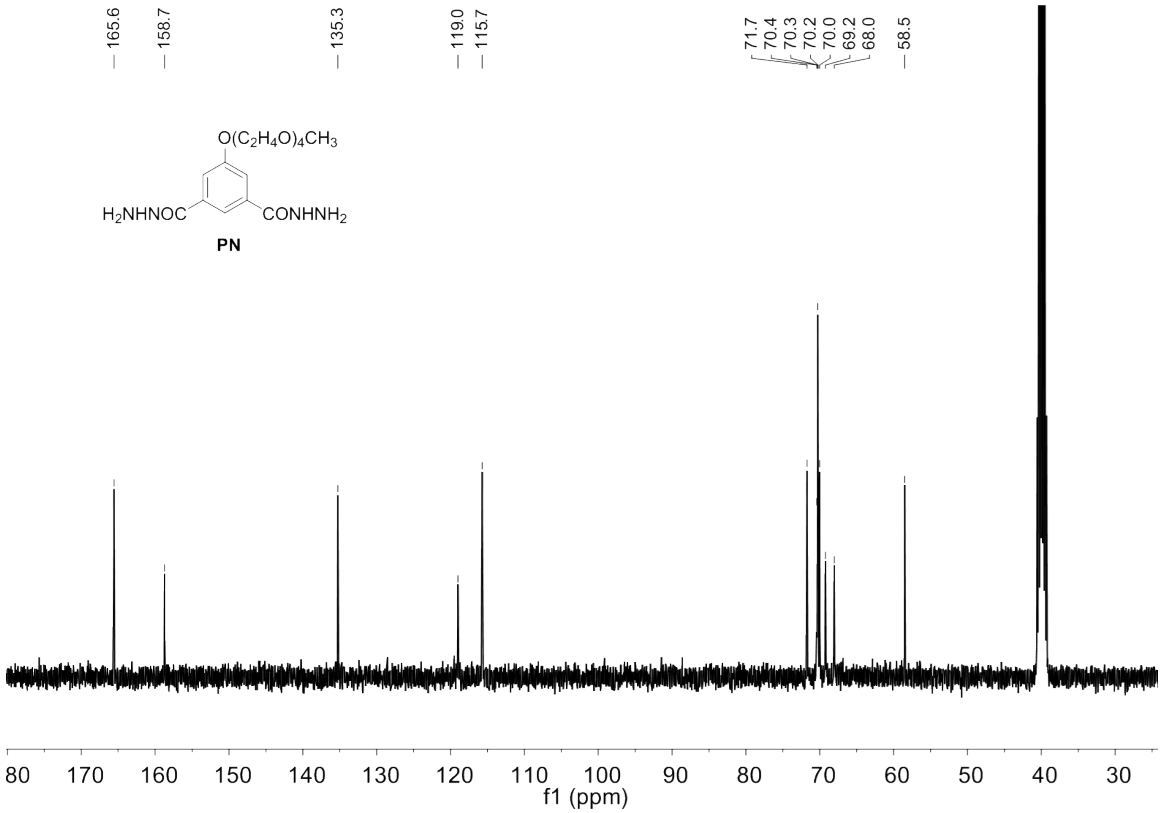

Figure S4. ^{13}C NMR spectrum of monomer **PN** in DMSO-d_6.

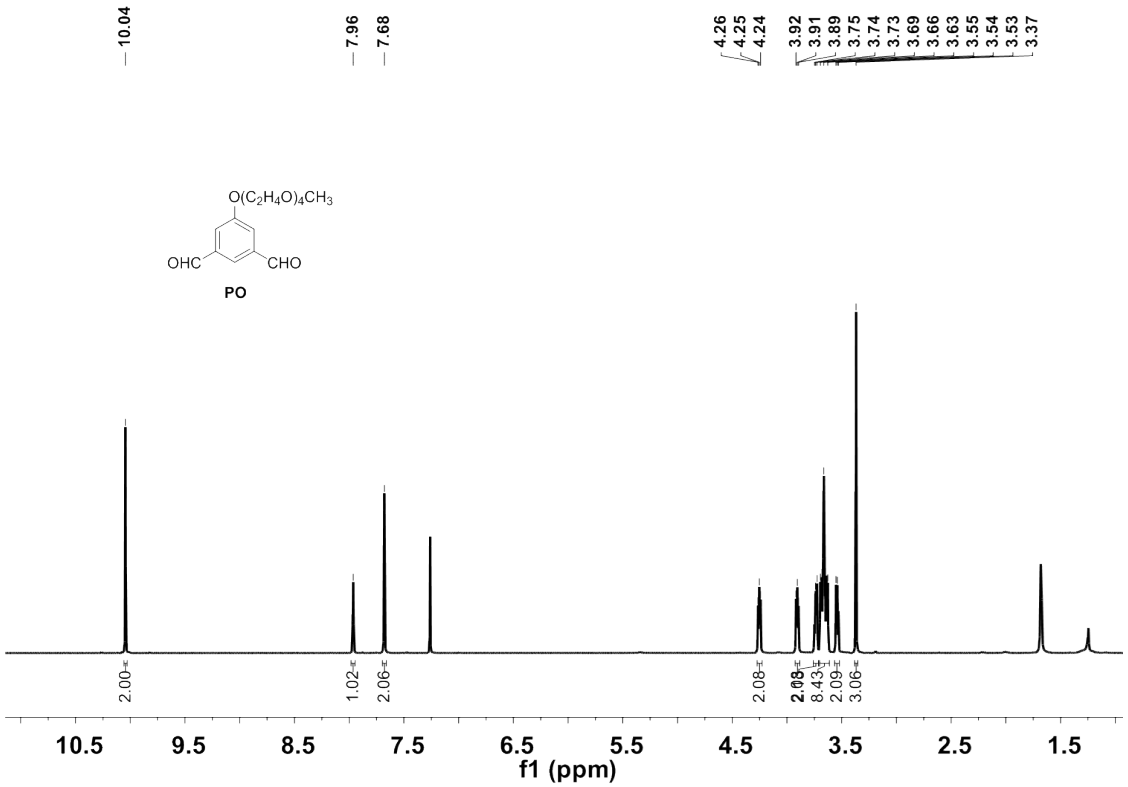

Figure S5. ^{1}H NMR spectrum of monomer **PO** in $CDCl_3$.

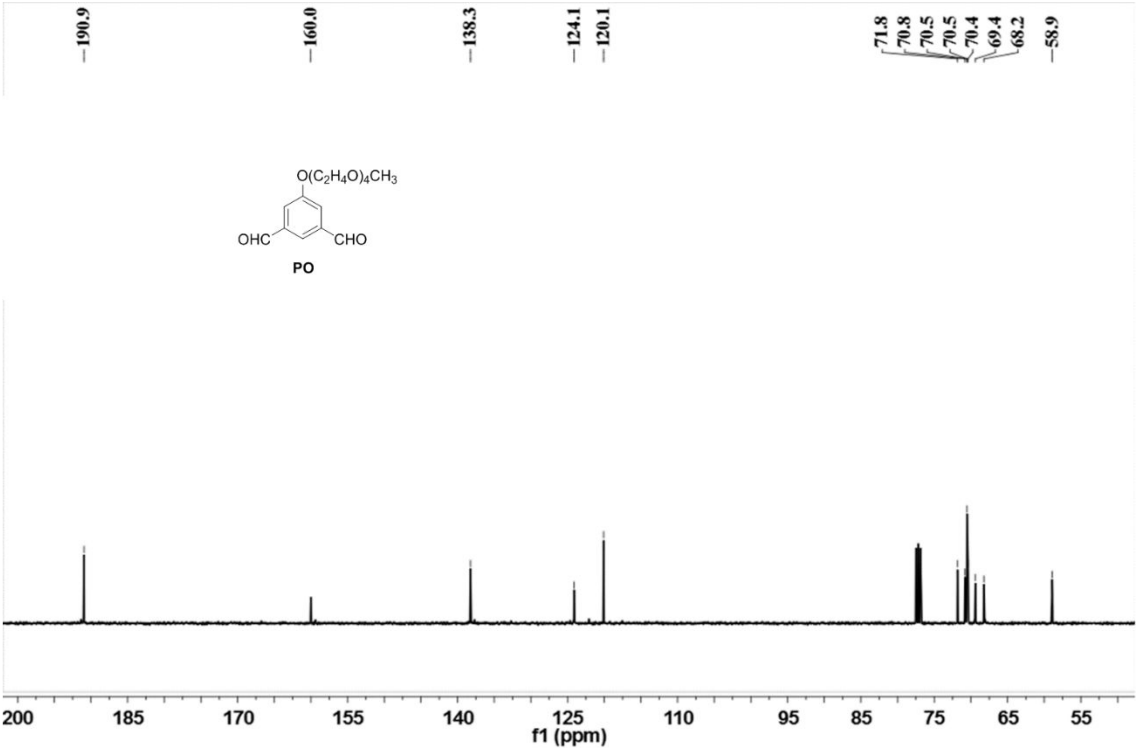

Figure S6. ^{13}C NMR spectrum of monomer **PO** in $CDCl_3$.

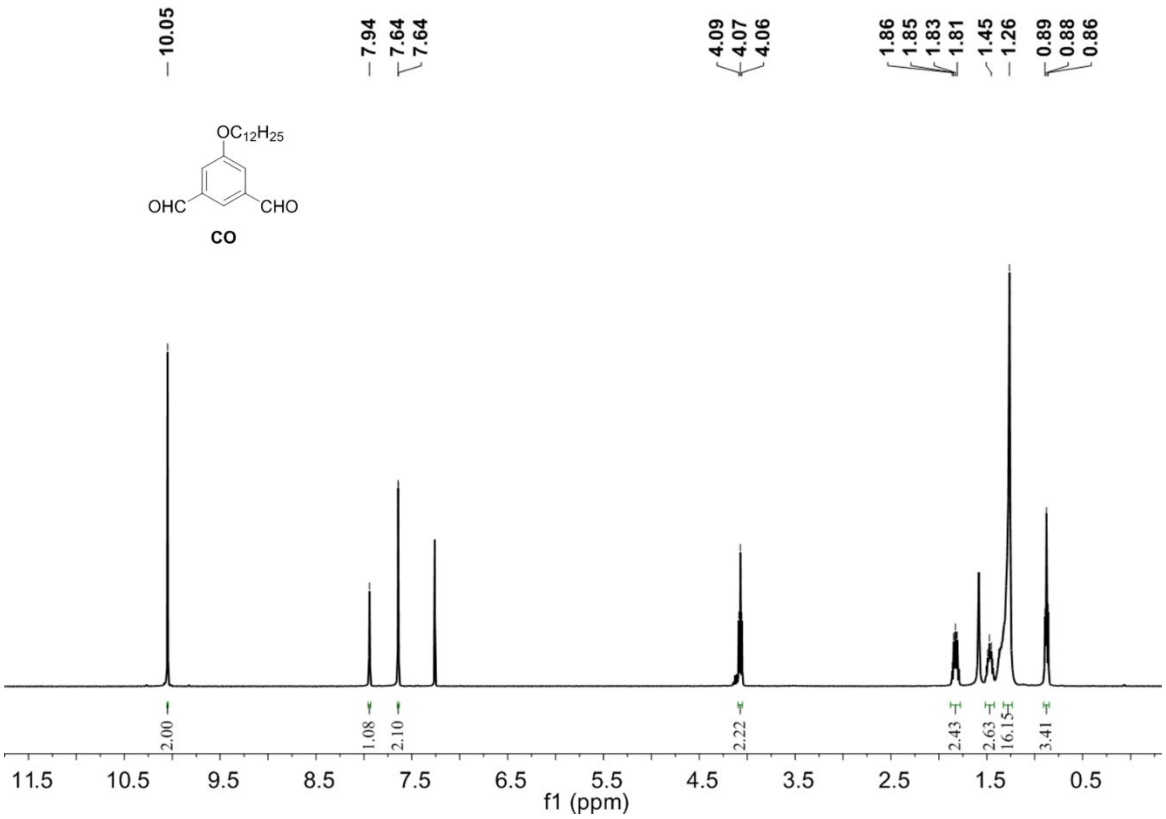

Figure S7. ^{1}H NMR spectrum of monomer **CO** in $CDCl_3$.

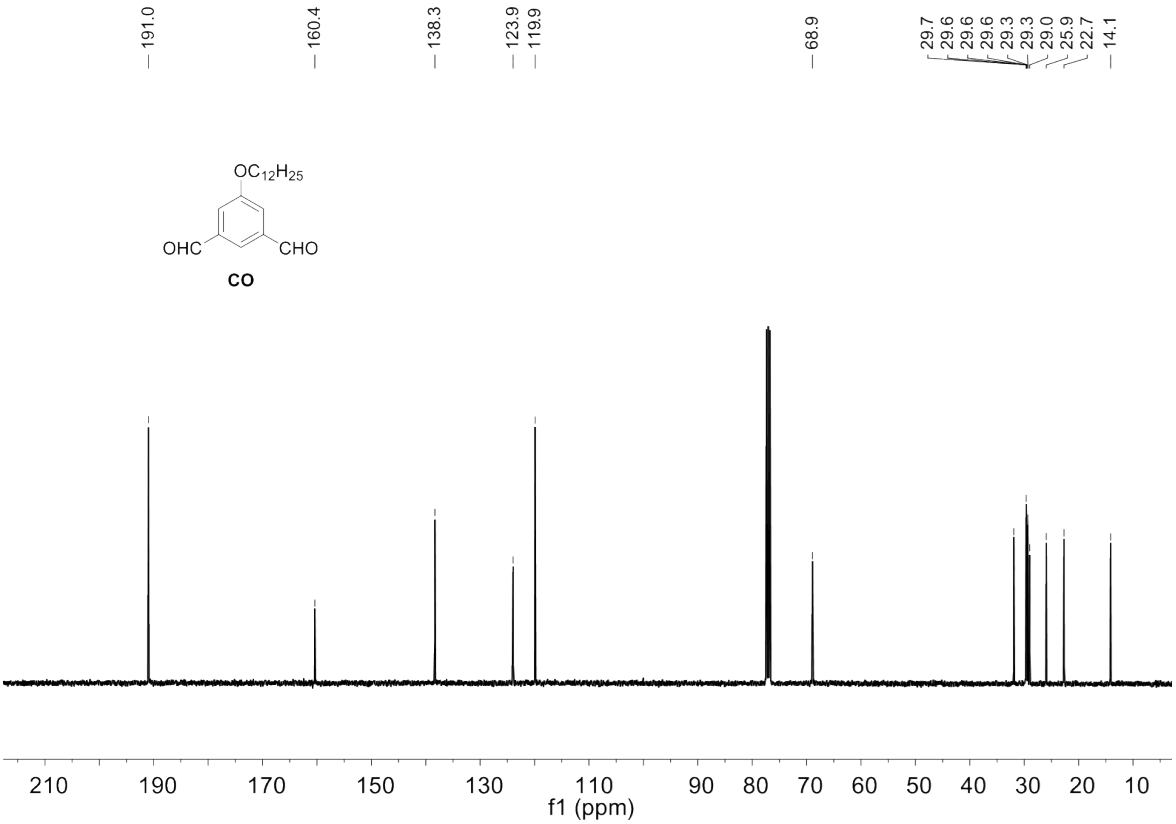

Figure S8. ^{13}C NMR spectrum of monomer **CO** in $CDCl_3$.

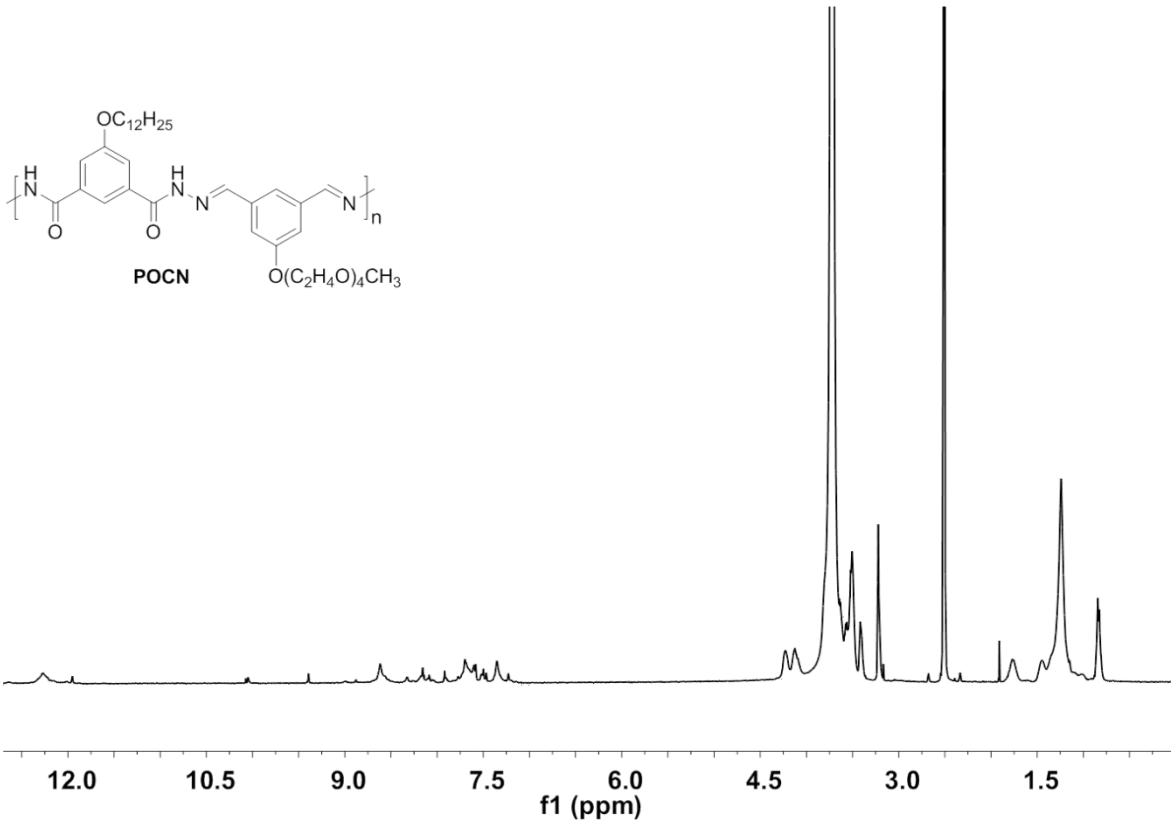

Figure S9. [1]H-NMR spectrum of polymer **POCN** in DMSO-d_6.

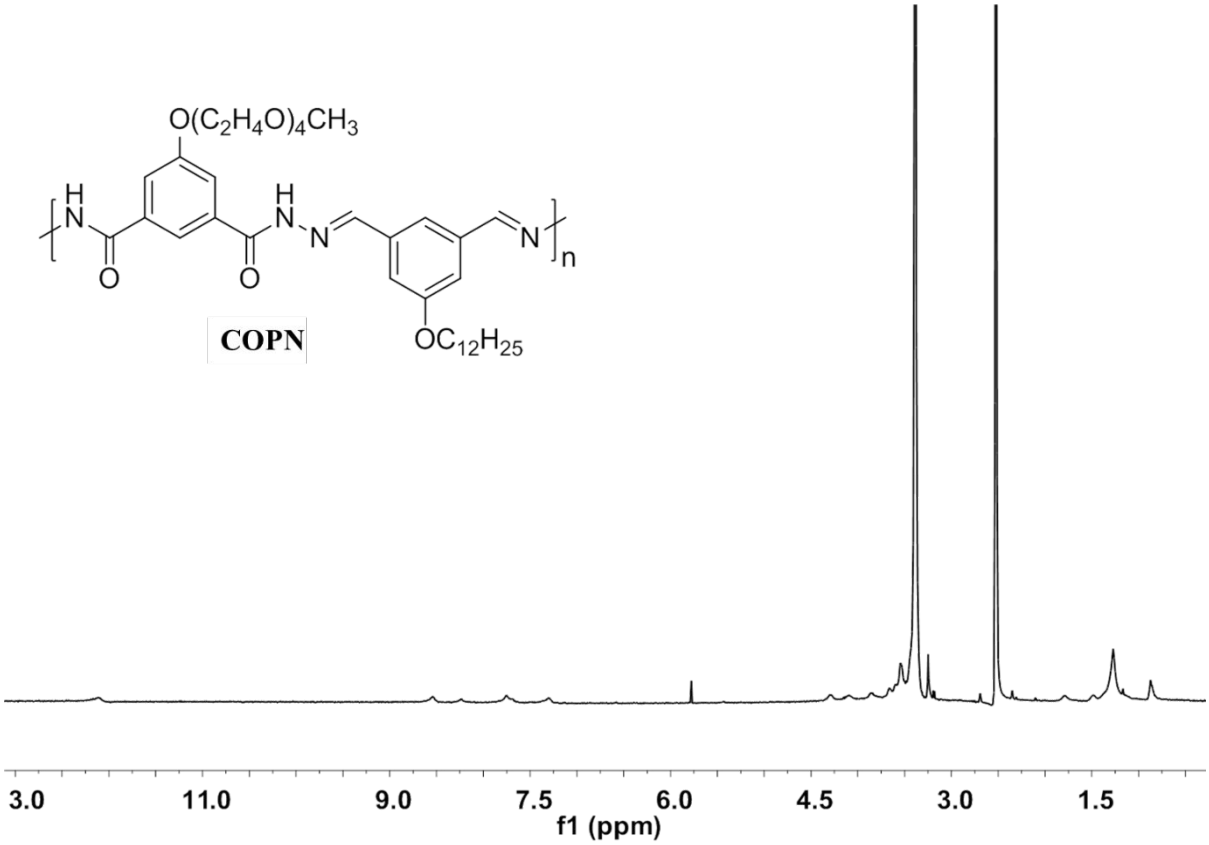

Figure S10. [1]H-NMR spectrum of polymer **COPN** in DMSO-d_6.

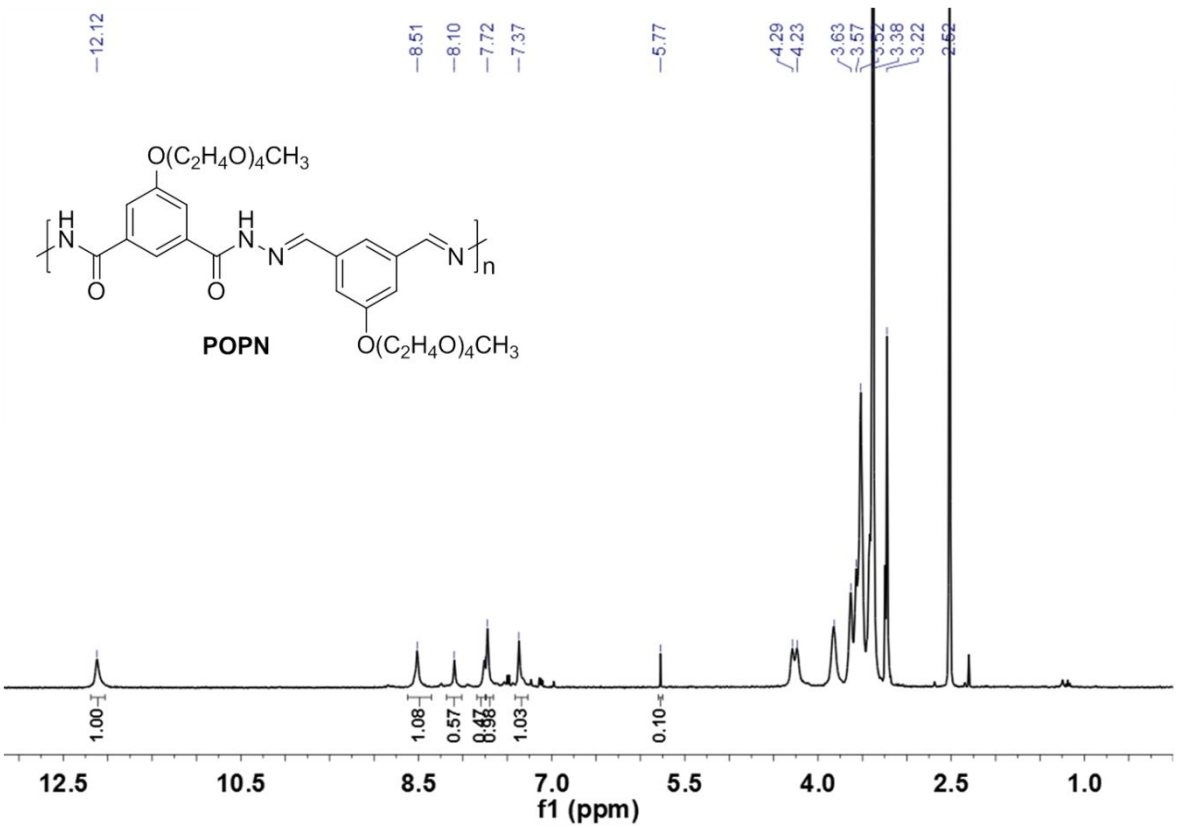

Figure S11. ^{1}H-NMR spectrum of polymer **POPN** in DMSO-d_6.

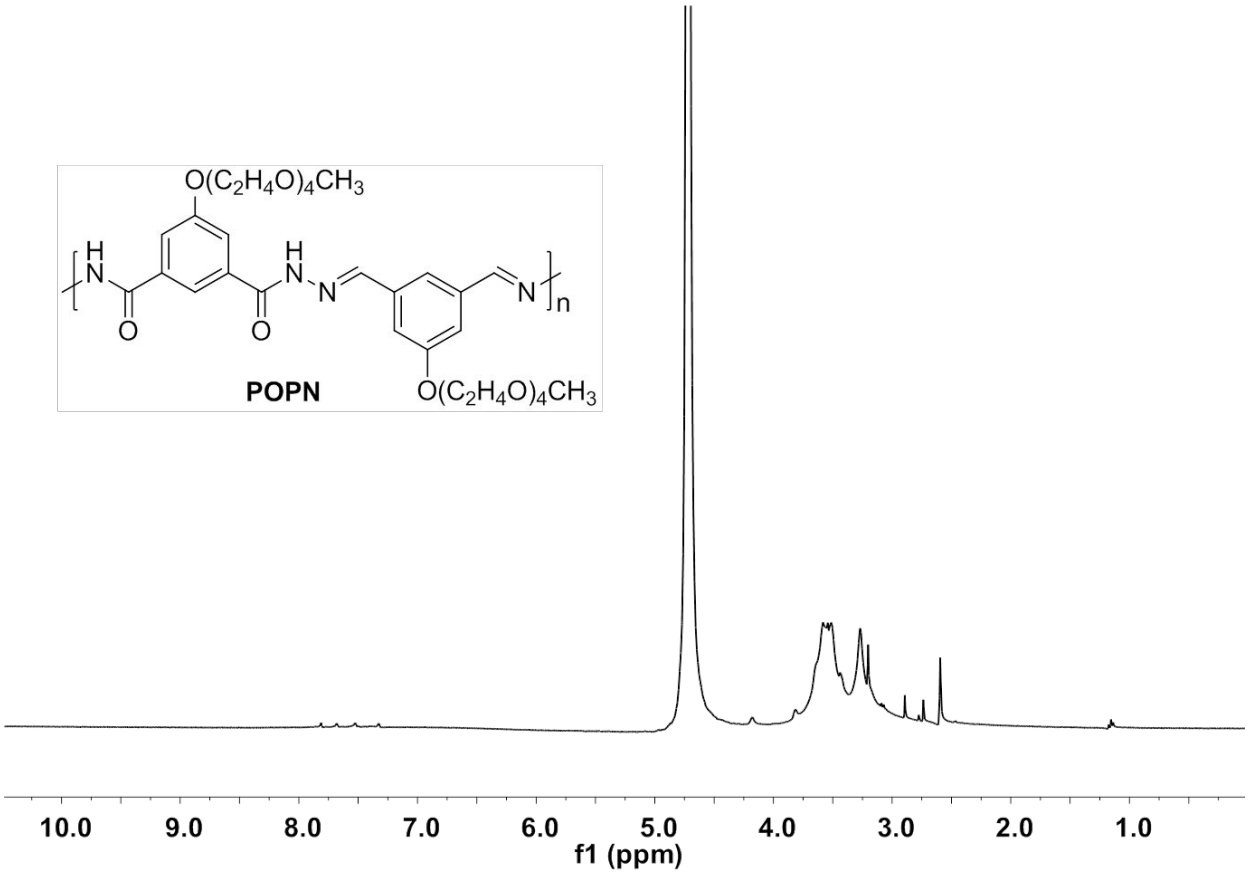

Figure S12. ^{1}H-NMR spectrum of polymer **POPN** in D_2O.

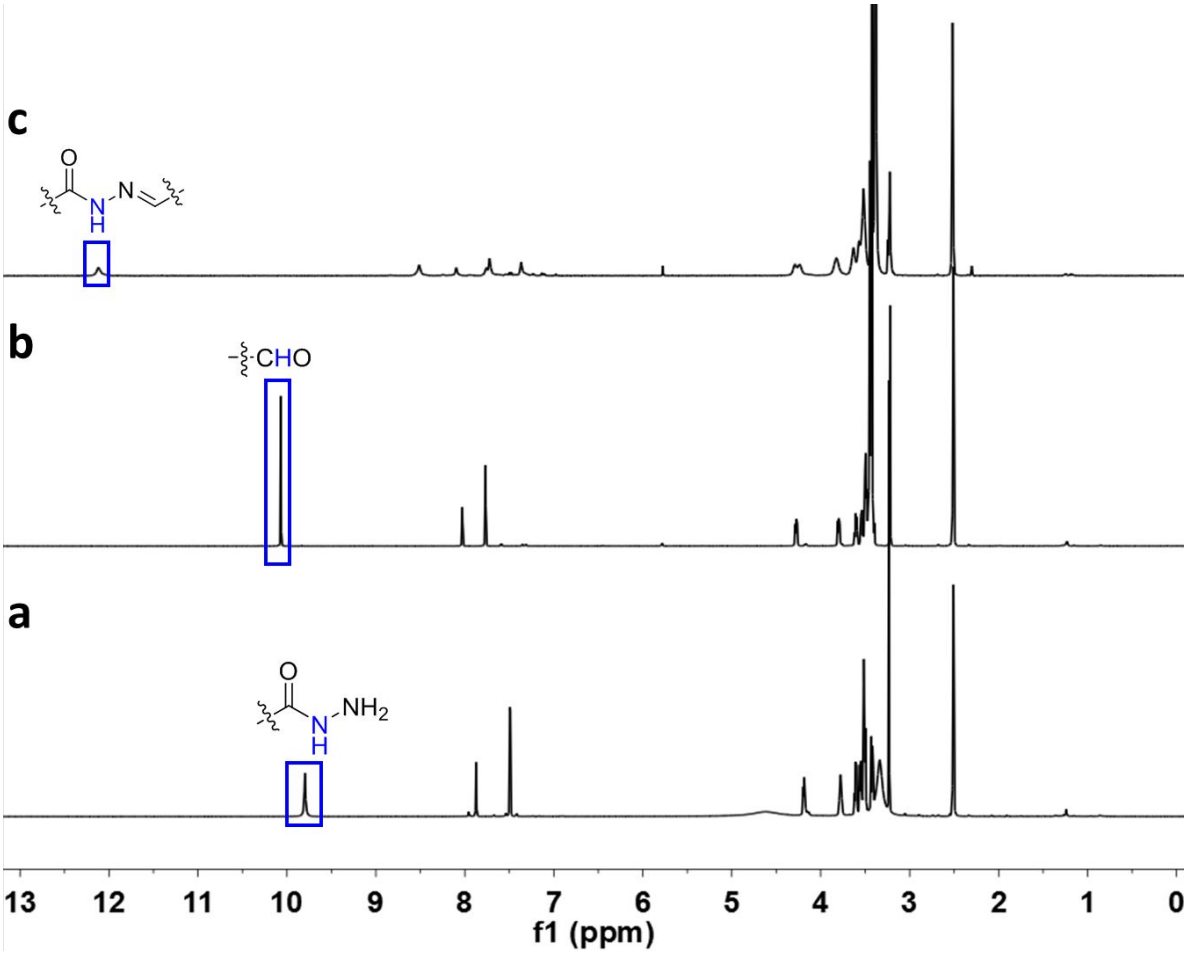

Figure S13. ^{1}H NMR spectra of **PN** (a), **PO** (b) and polymer **POPN** (c) in DMSO-d_6.

Gel permeation chromatography analysis

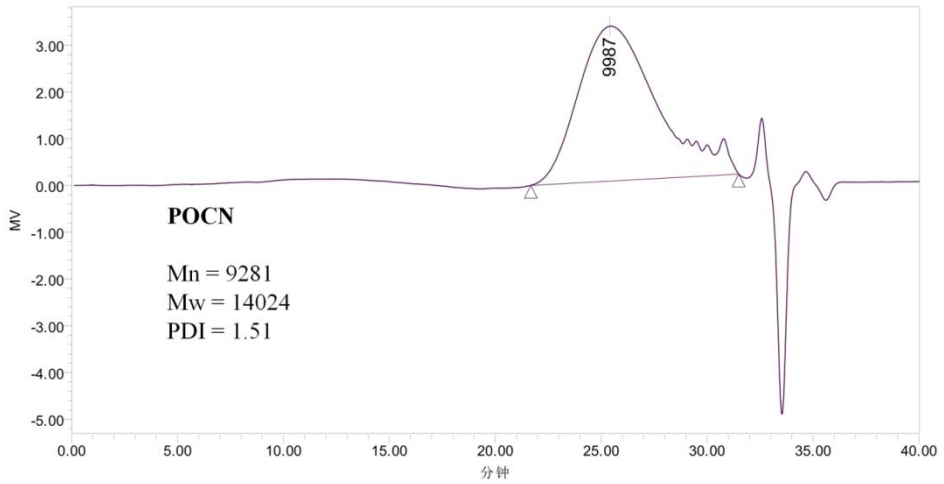

Figure S14. GPC trace of **POCN**.

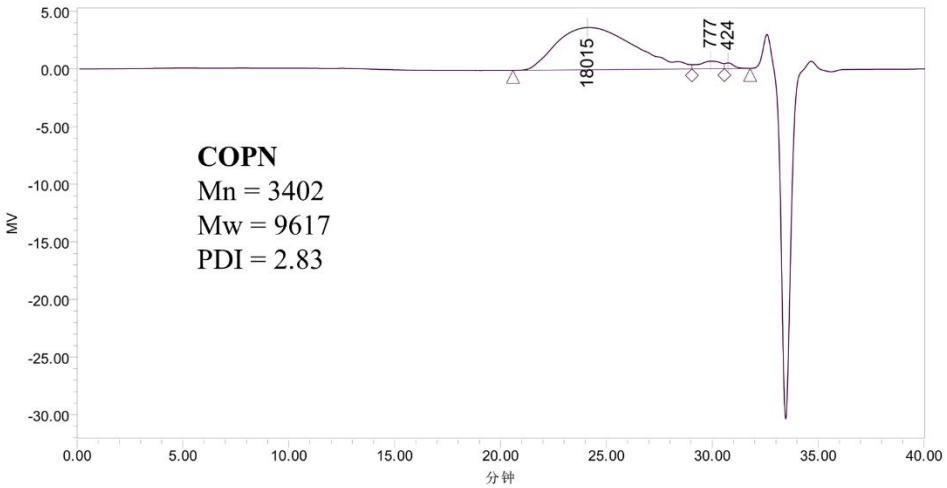

Figure S15. GPC trace of **COPN**.

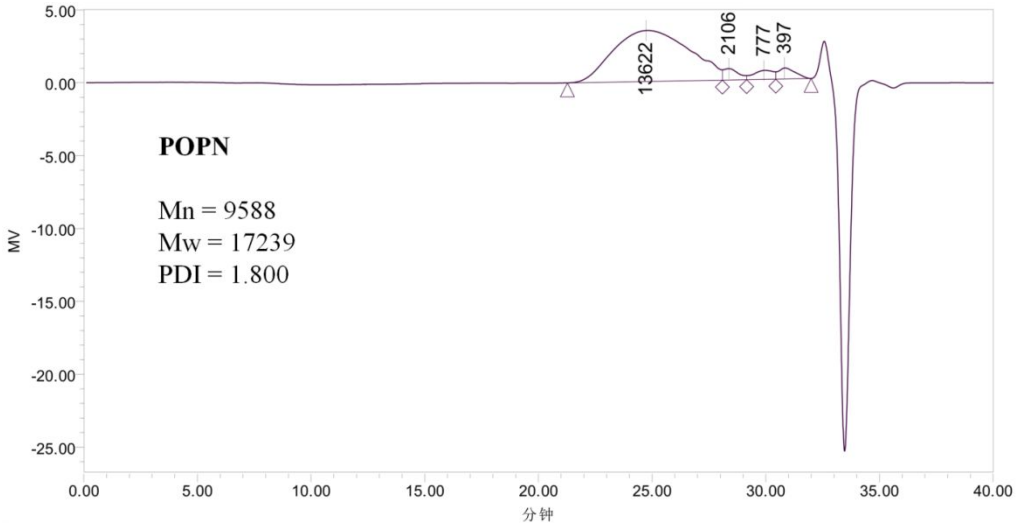

Figure S16. GPC trace of **POPN**.

2. Temperature Responsiveness Studies of POCN/COPN

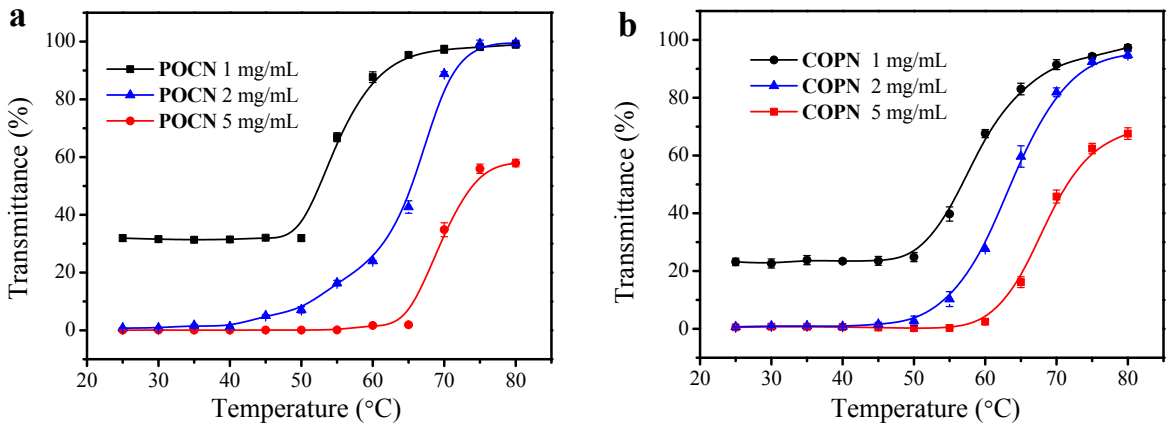

Figure S17. Temperature dependence of the transmittance of **POCN** (a) and **COPN** (b) at 1.0, 2.0, and 5.0 mg/mL in DMSO.

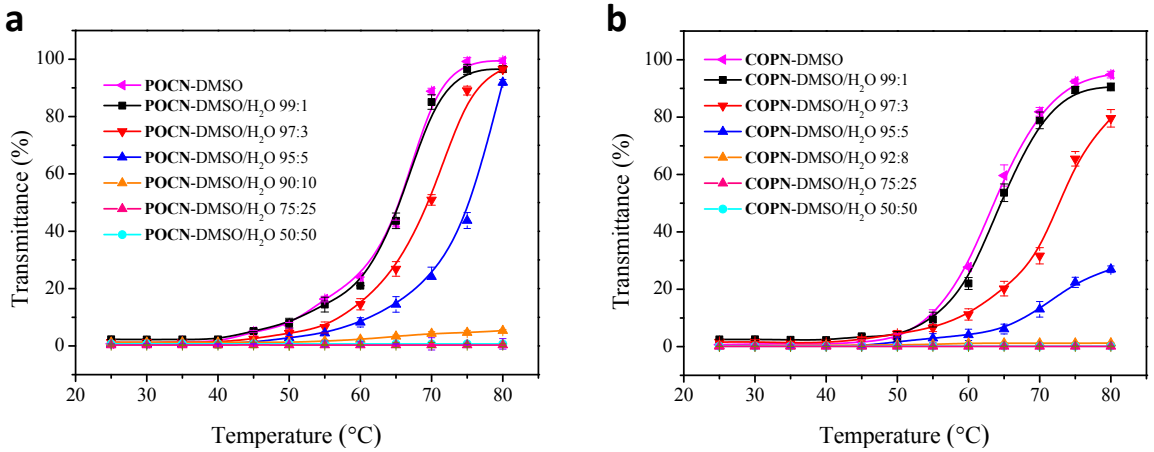

Figure S18. Temperature dependence of the transmittance of **POCN** (a, 2.0 mg/mL) and **COPN** (b, 2.0 mg/mL) in DMSO/water (v/v).

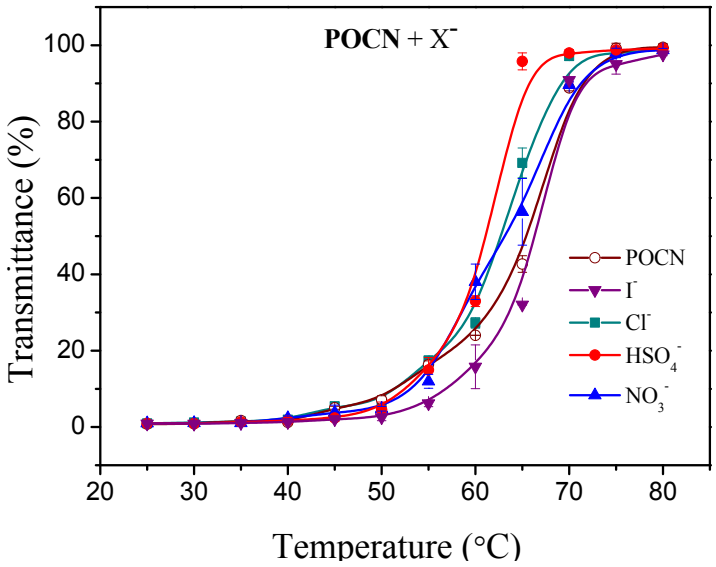

Figure S19. Temperature dependence of the transmittance of **POCN** (2.0 mg/mL) in the presence of various anions (8.0 mM).

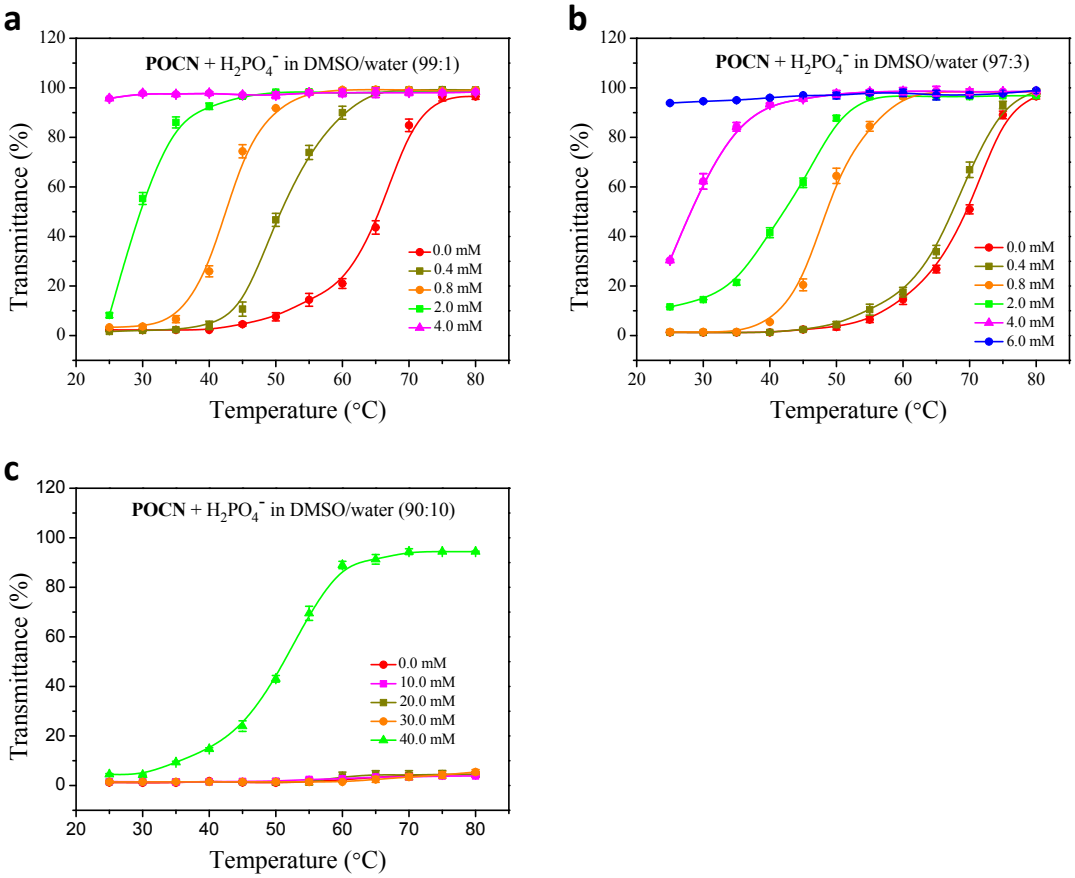

Figure S20. Temperature dependence of the transmittance of **POCN** (2.0 mg/mL) in the presence of different concentrations of $H_2PO_4^-$ in DMSO/water (v/v). (a) 99:1, (b) 97:3, (c) 90:10.

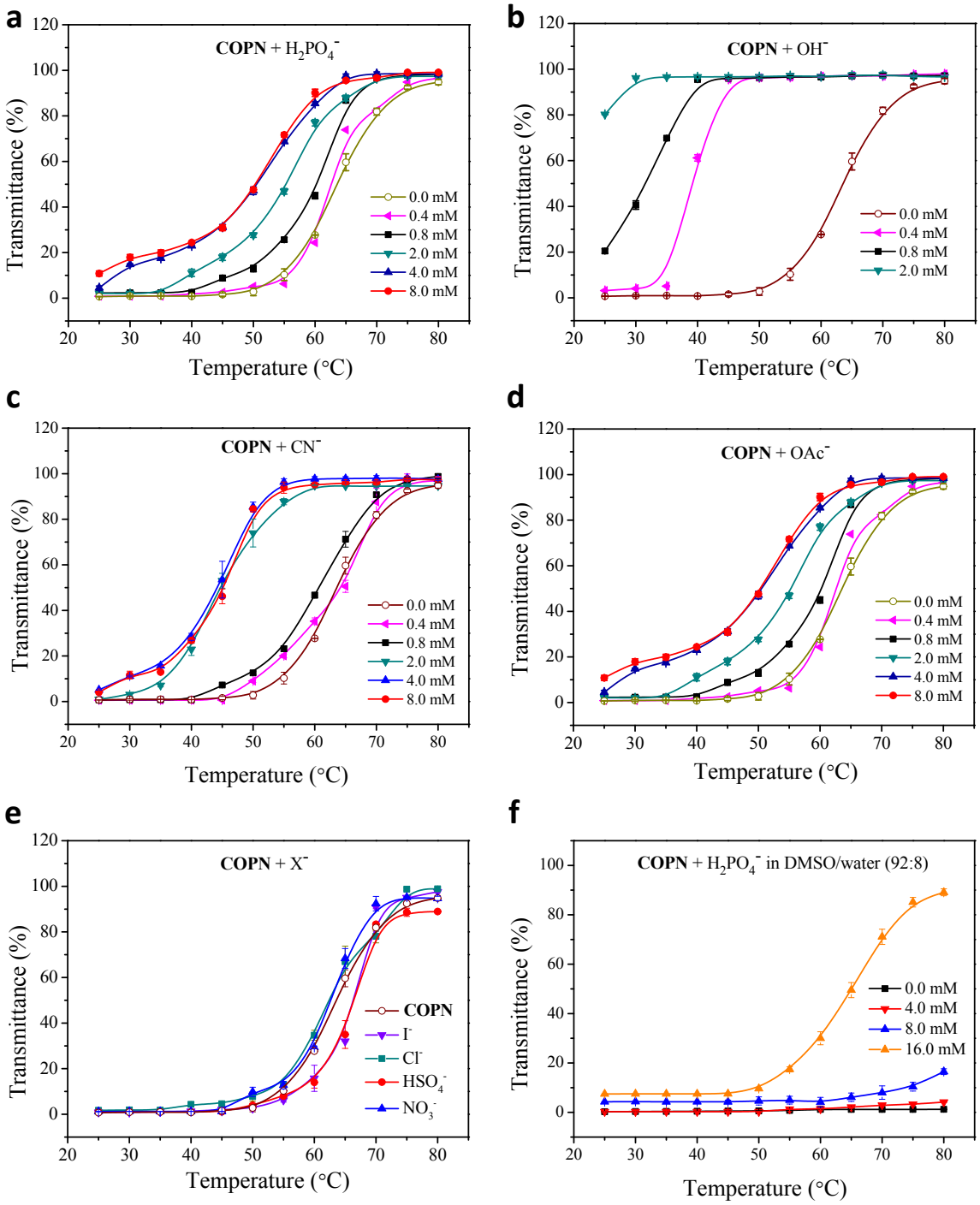

Figure S21. Temperature dependence of the transmittance of **COPN** (2.0 mg/mL) in the presence of different concentrations of (a) $H_2PO_4^-$, (b) OH^-, (c) CN^-, (d) OAc^-, (e) other anions (8 mM) in DMSO. (f) Temperature dependence of the transmittance of **COPN** (2.0 mg/mL) in the presence of different concentration $H_2PO_4^-$ in DMSO/water 92:8 (v/v).

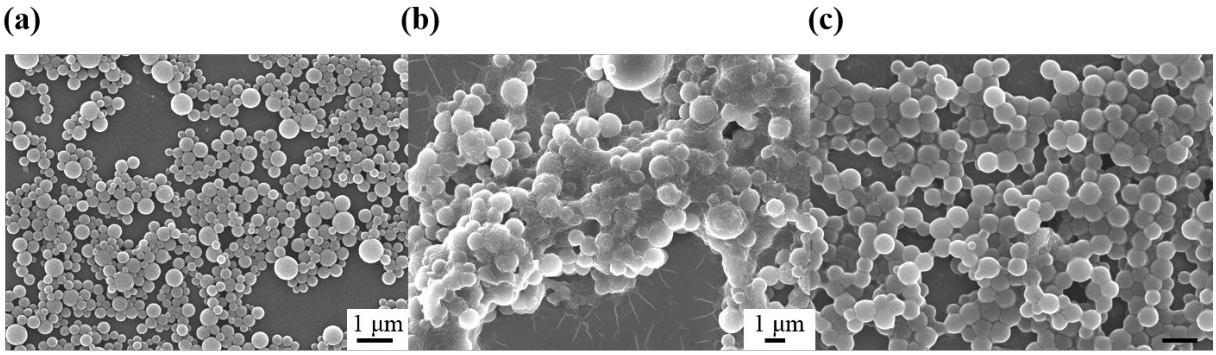

Figure S22. SEM images (a) **POCN** (2.0 mg/mL) in DMSO, (b) **POCN** (2.0 mg/mL) in 4:1 DMSO/H_2O, and (c) **COPN** (2.0 mg/mL) in DMSO.

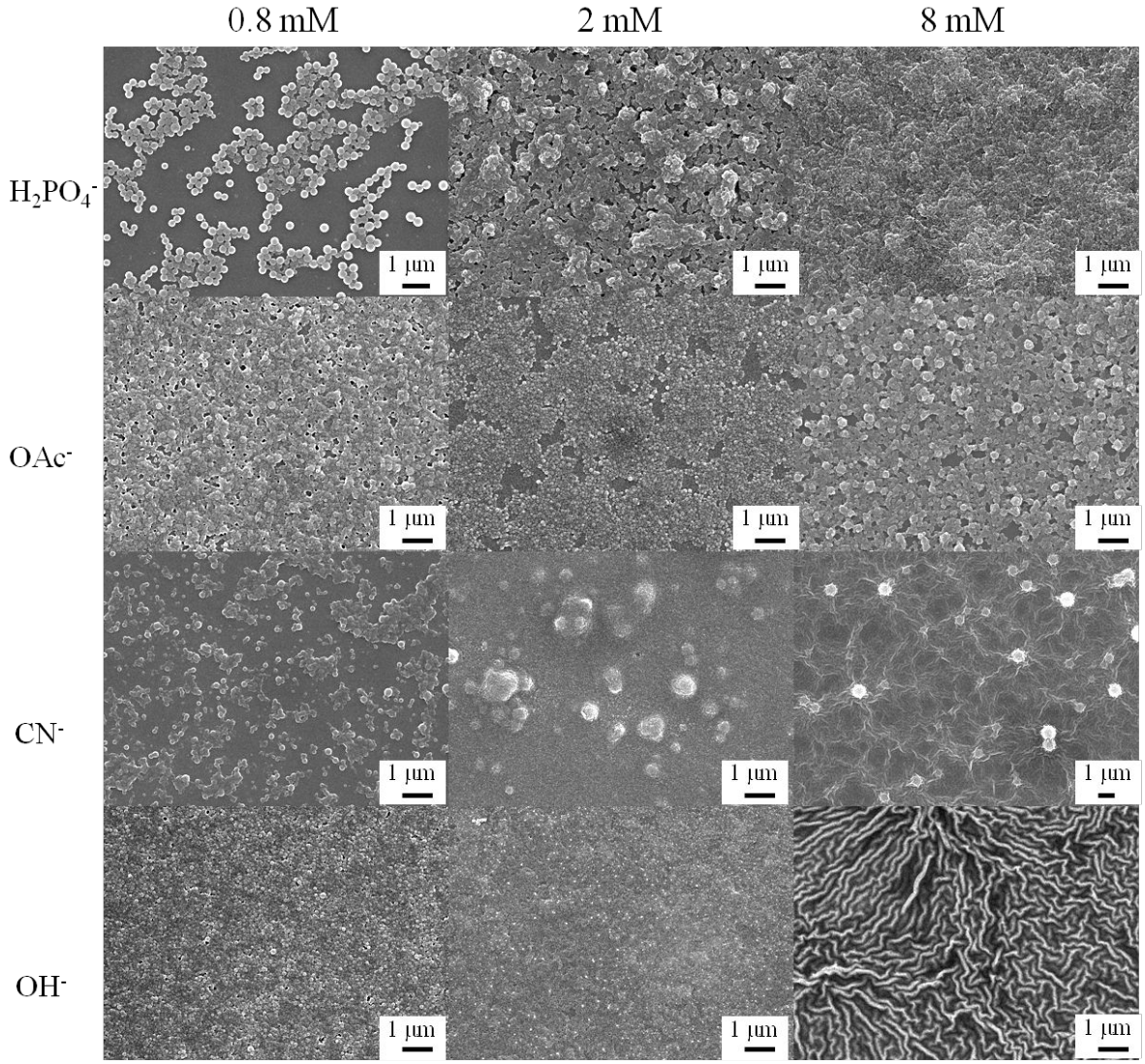

Figure S23. SEM images of **POCN** (2.0 mg/mL) in presence of different concentrations of $H_2PO_4^-$, OAc^-, CN^-, and OH^-.

3. Temperature Responsiveness Studies of POPN

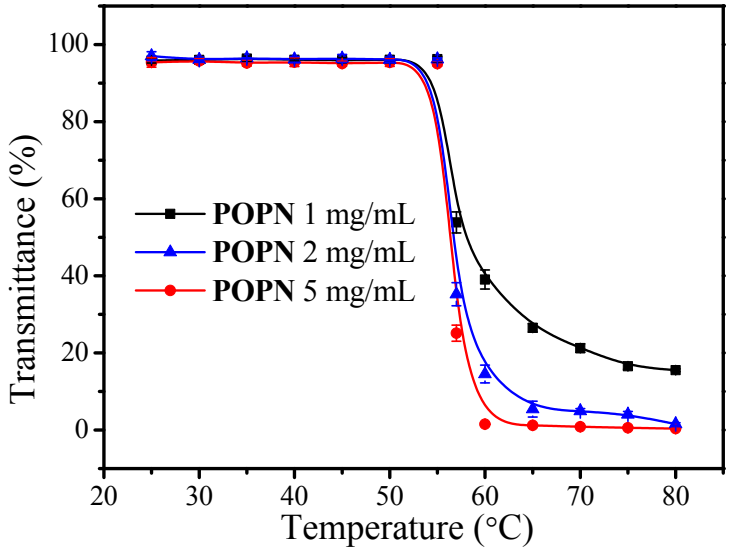

Figure S24. Temperature dependence of the transmittance of **POPN** at 1.0, 2.0, and 5.0 mg/mL in water.

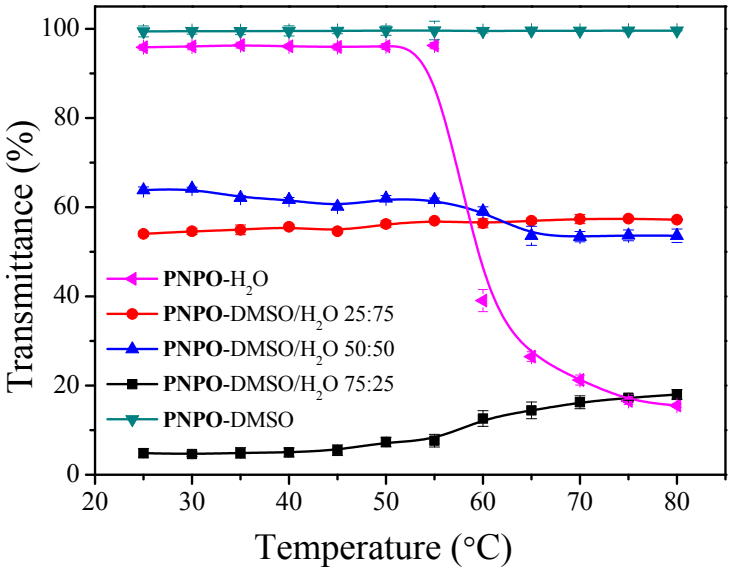

Figure S25. Temperature dependence of the transmittance of **POPN** (2.0 mg/mL) in DMSO/H_2O (v/v).

4. Dynamic Covalent Exchange

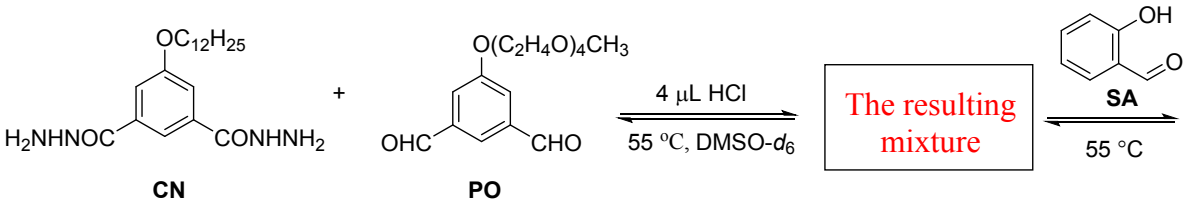

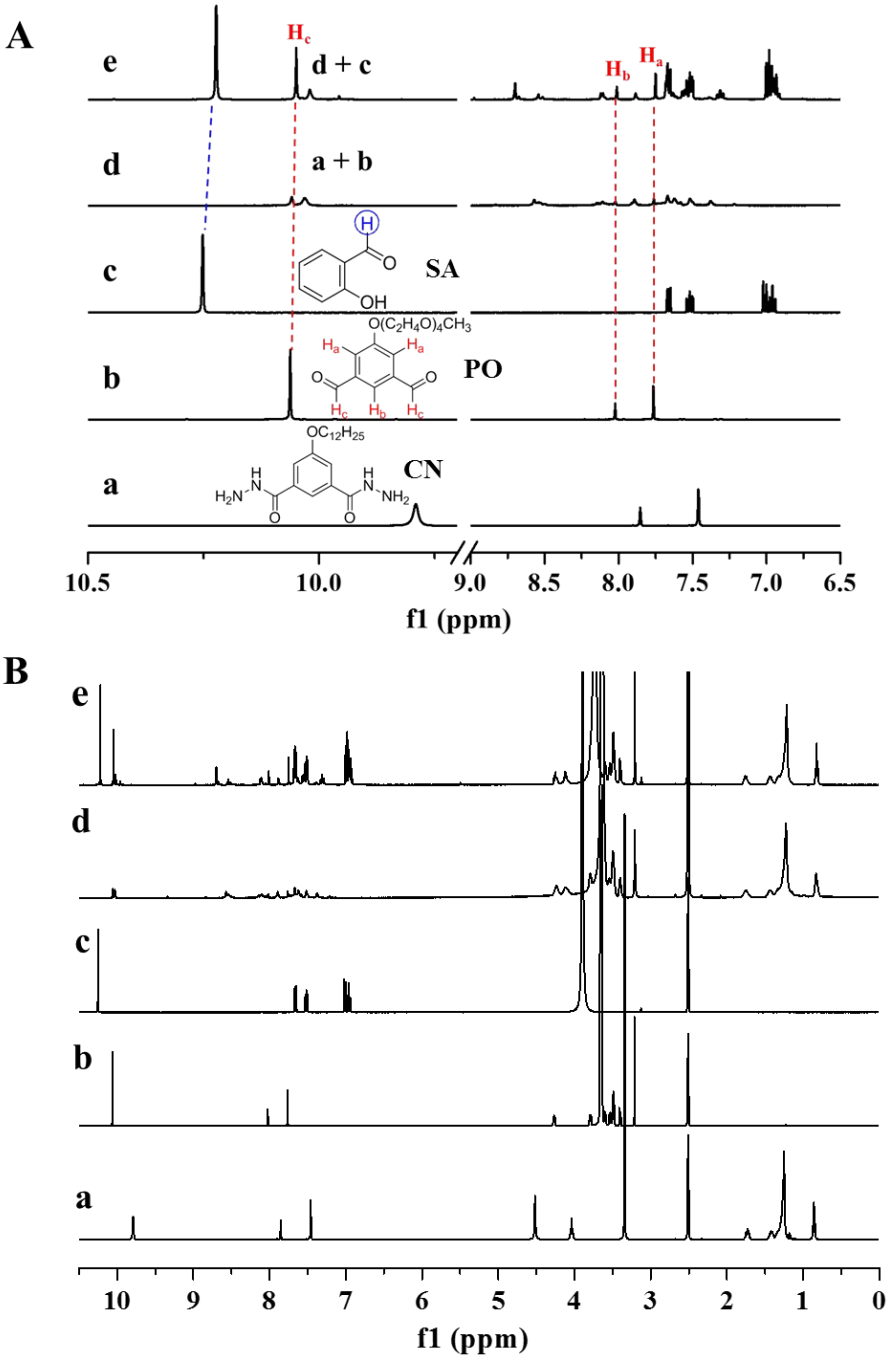

Figure S26. (A) Dynamic component exchange between **PO** and **SA** in the presence of HCl in DMSO-d_6: **CN** (a); **PO** (b); **SA** (c); the reaction of **CN** with **PO** in the presence of HCl (d); the addition of **SA** into panel d (e); (B) The full ^{1}H NMR spectra of A. This figure shows the NMR spectra of entry 1 in Table 1 in the main text.

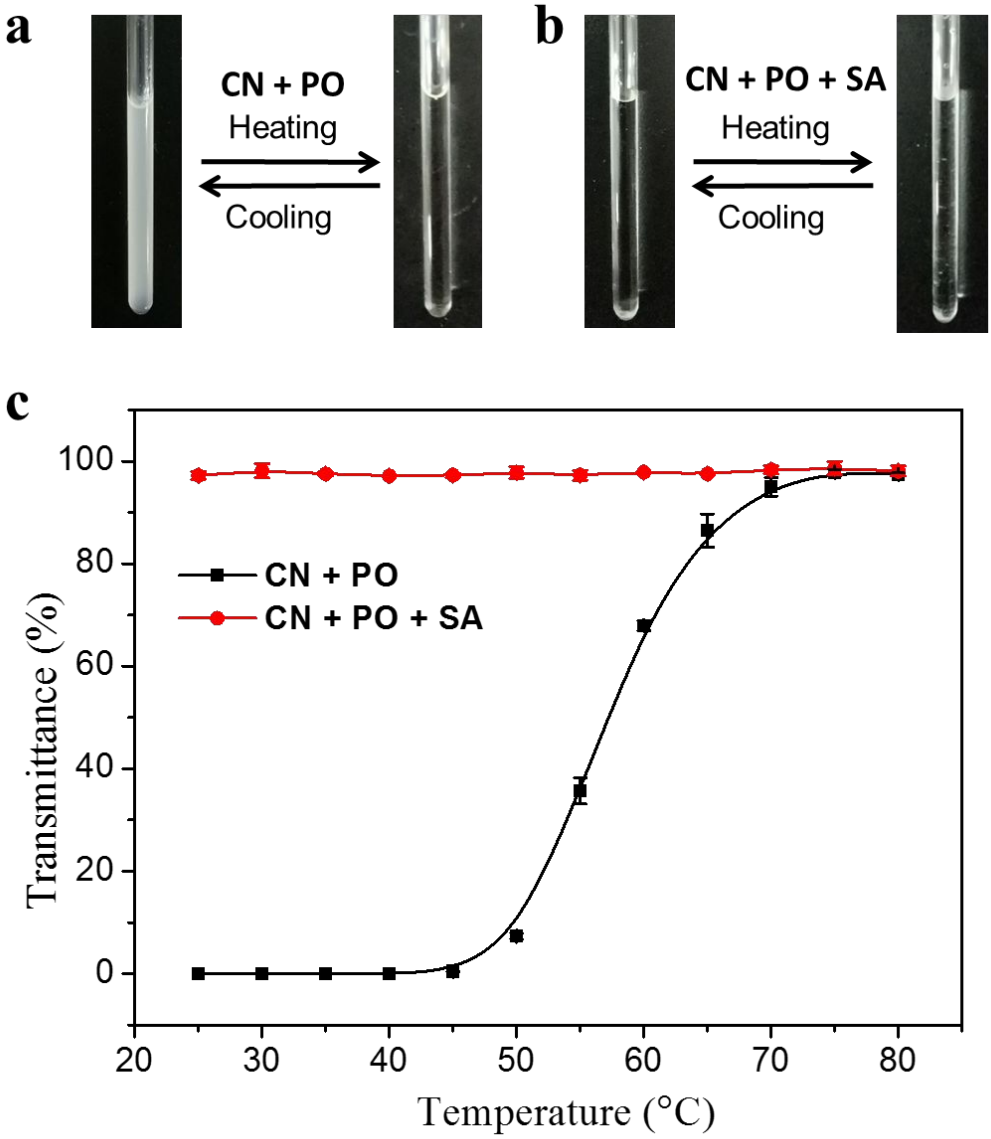

Figure S27. Photographs (a, b) and temperature dependence of the transmittance (c) of dynamic reactions in Figure S26 during a heating/cooling process.

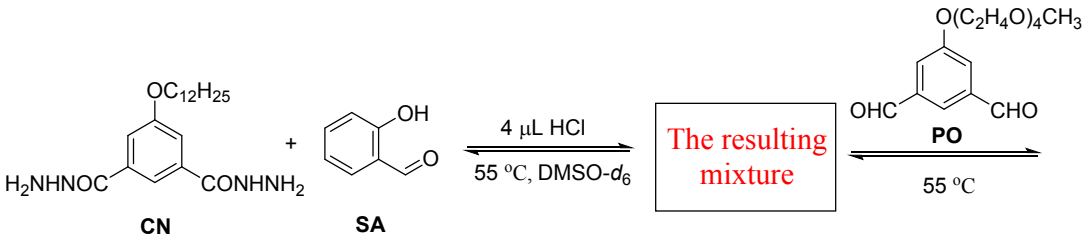

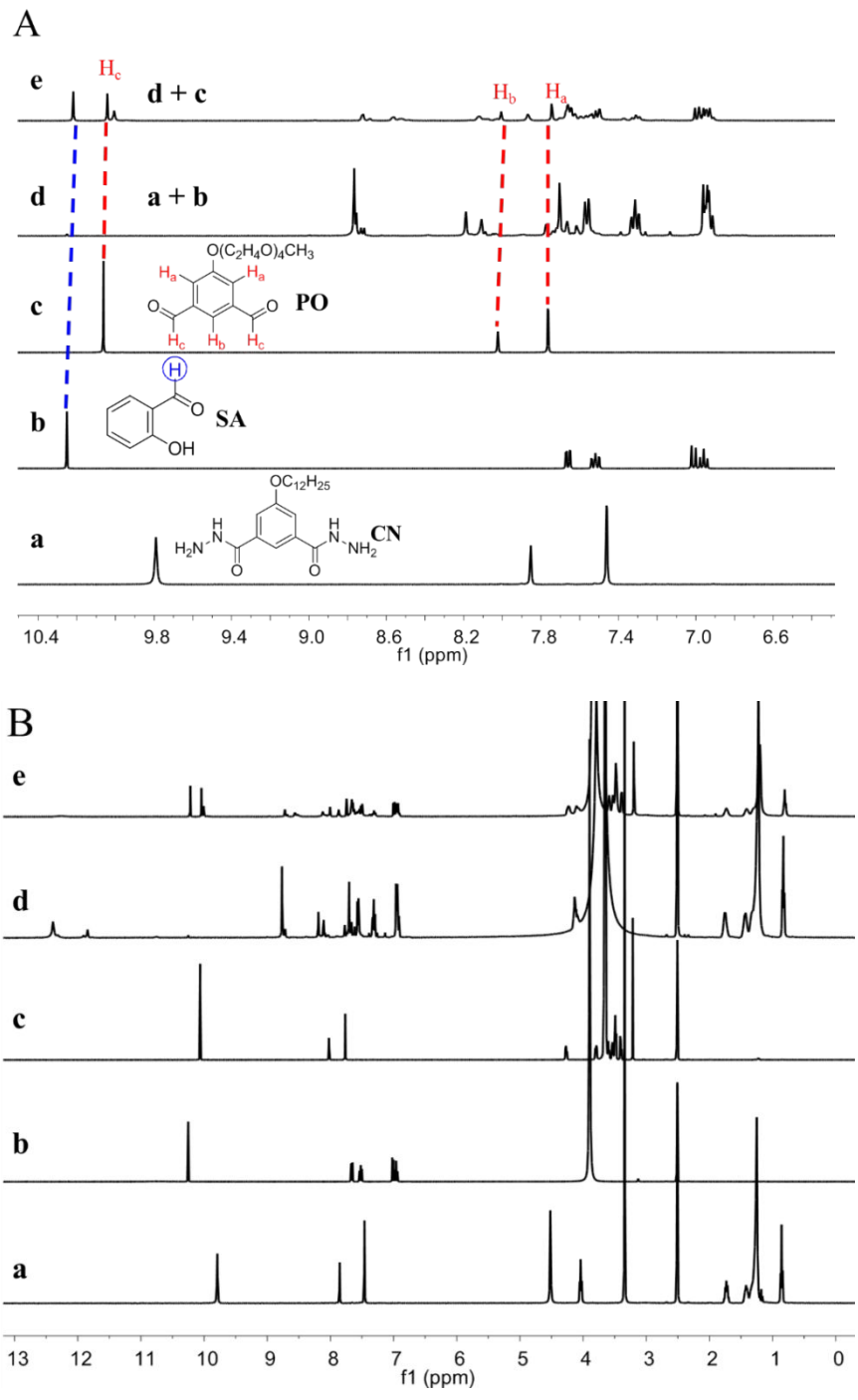

Figure S28. (A) Dynamic component exchange between **SA** and **PO** in the presence of HCl in DMSO-d_6: **CN** (a); **SA** (b); **PO** (c); the reaction of **CN** with **SA** in the presence of HCl (d); the addition of **PO** into panel d (e); (B) The full ^{1}H NMR spectra of A. This figure shows the NMR spectra of entry 2 in Table 1 in the main text.

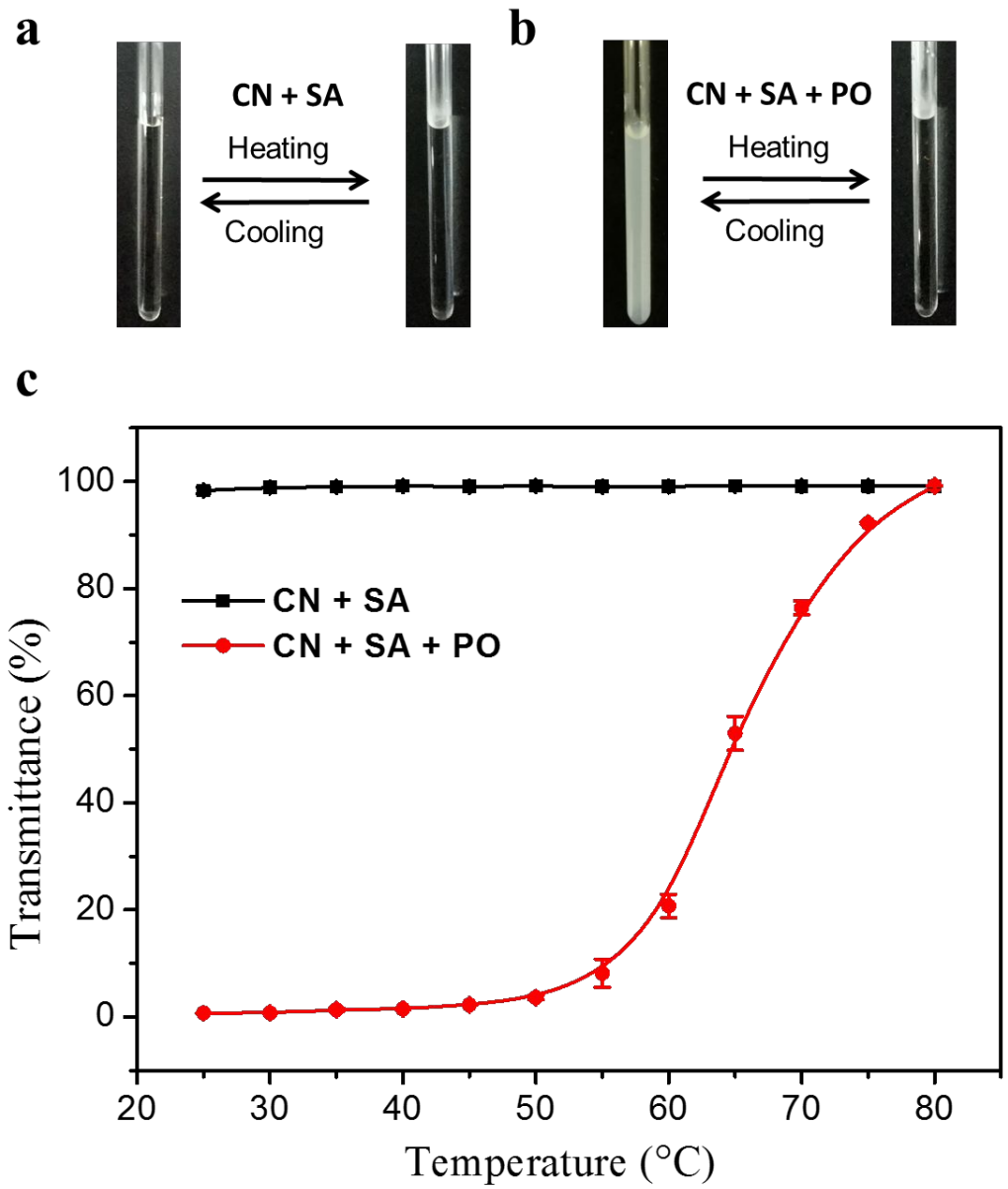

Figure S29. Photographs (a, b) and temperature dependence of the transmittance (c) of dynamic reactions in Figure S28 during a heating/cooling process.

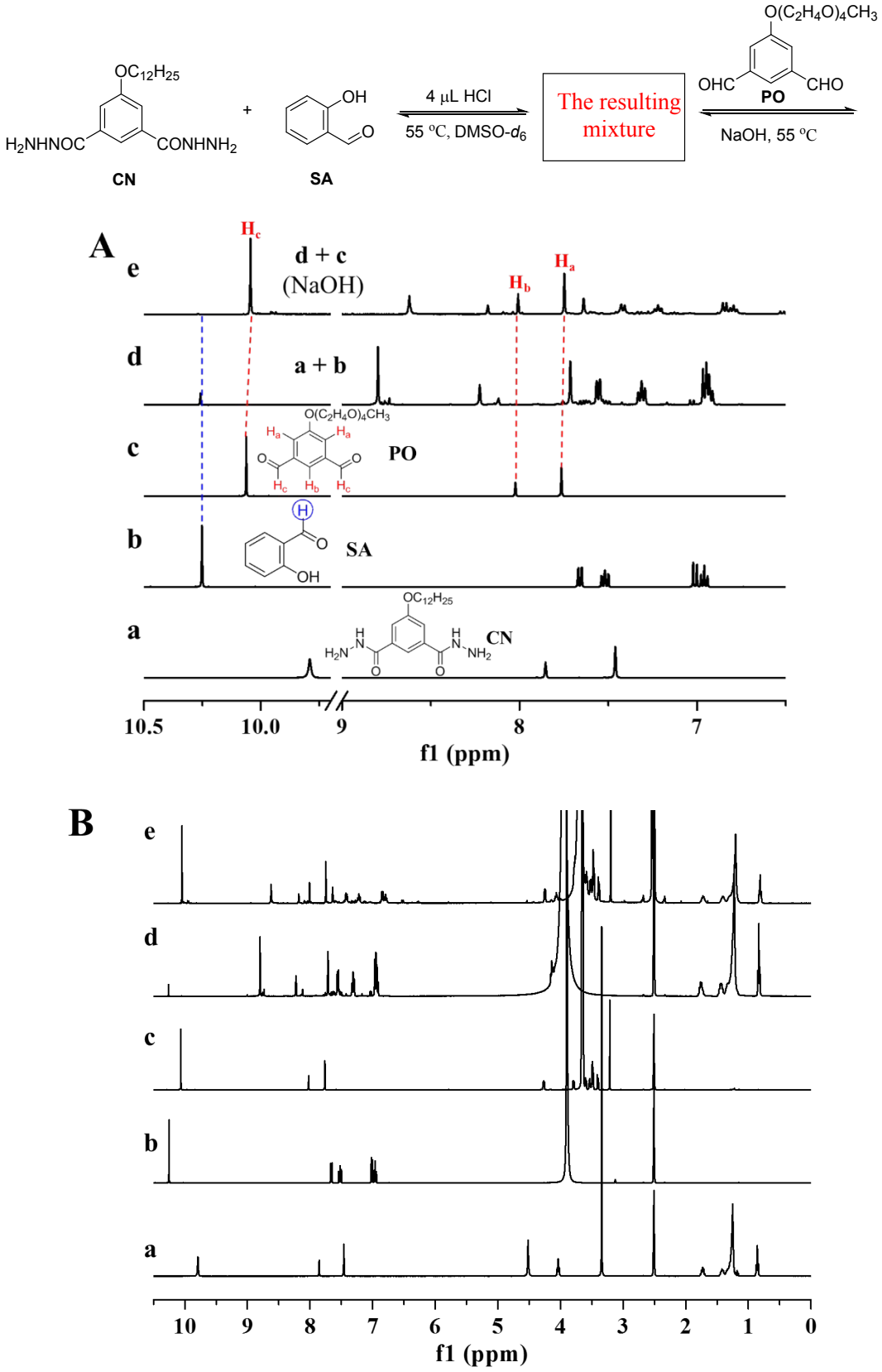

Figure S30. (A) Dynamic component exchange between **SA** and **PO** under neural condition in DMSO-d_6: **CN** (a); **SA** (b); **PO** (c); the reaction of **CN** with **SA** in the presence of HCl (d); the addition of **PO** into panel d with addition NaOH (e); (B) The full ^{1}H NMR spectra of A.

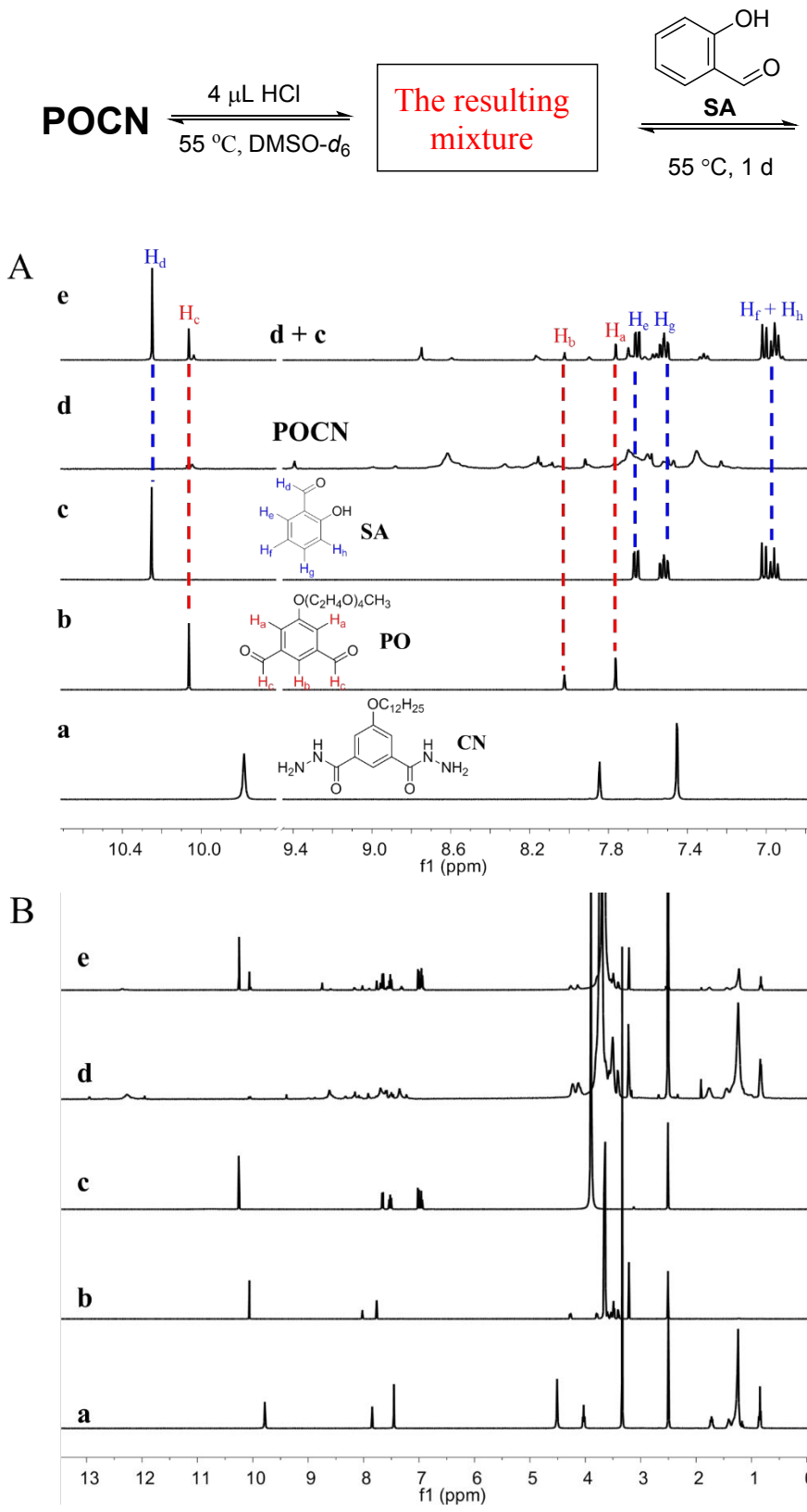

Figure S31. (A) Dynamic component exchange between **PO** and **SA** in the presence of HCl in DMSO-d_6: **CN** (a); **PO** (b); **SA** (c); **POCN** (d); the addition of **SA** into panel d (e); (B) The full ^{1}H NMR spectra of A. This figure shows the NMR spectra of entry 3 in Table 1 in the main text.

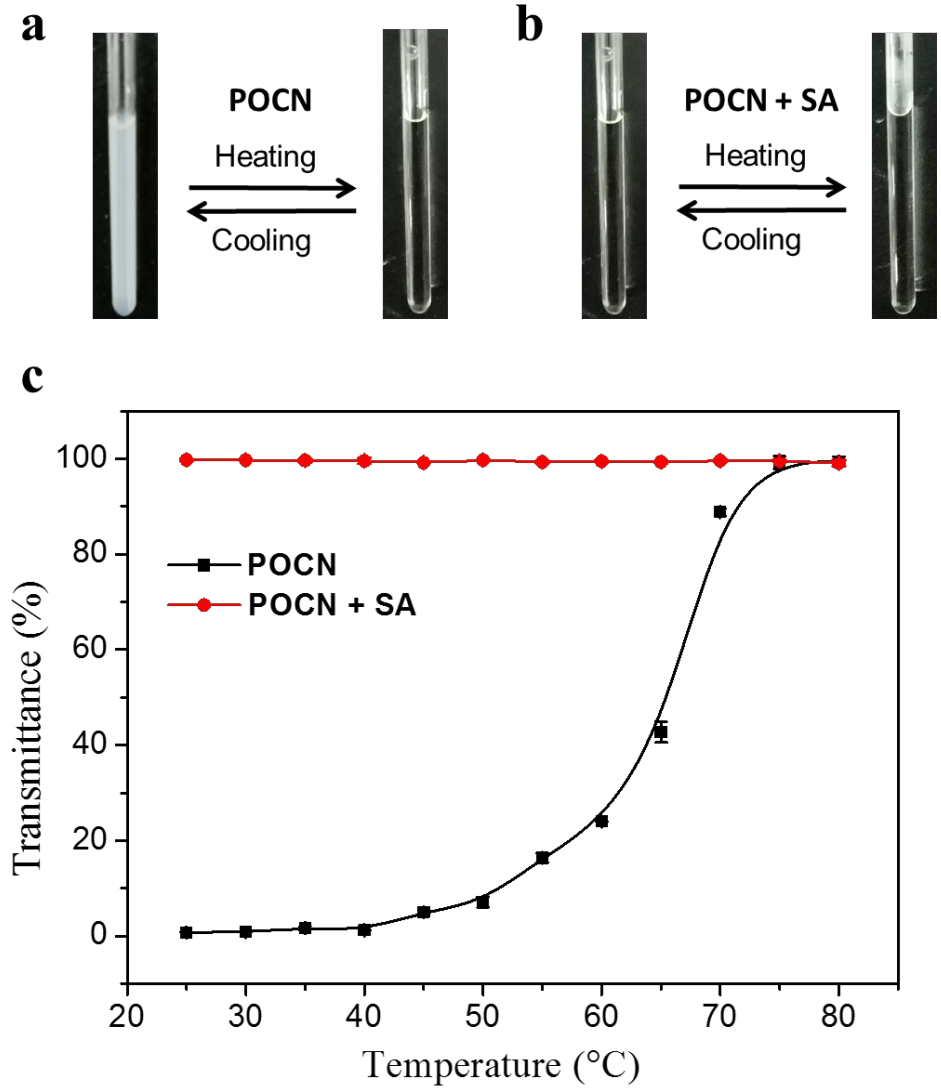

Figure S32. Photographs (a, b) and temperature dependence of the transmittance (c) of dynamic reactions in Figure S31 during a heating/cooling process.

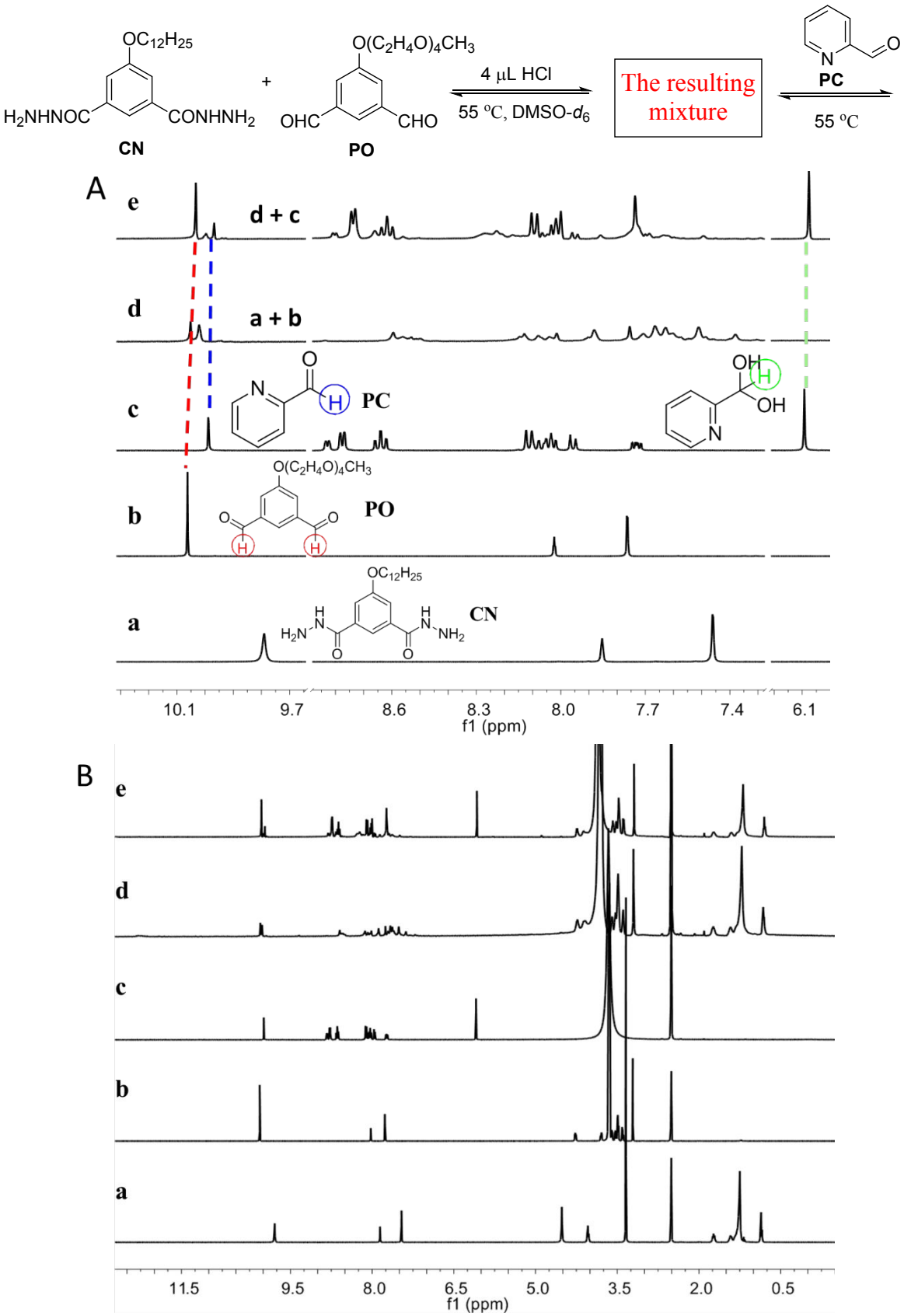

Figure S33. (A) Dynamic component exchange between **PO** and **PC** in the presence of HCl in DMSO-d_6: **CN** (a); **PO** (b); **PC** (c); the reaction of **CN** with **PO** in the presence of HCl (d); the addition of **PC** into panel d (e); (B) The full ^{1}H NMR spectra of **A**. This figure shows the NMR spectra of entry 4 in Table 1 in the main text.

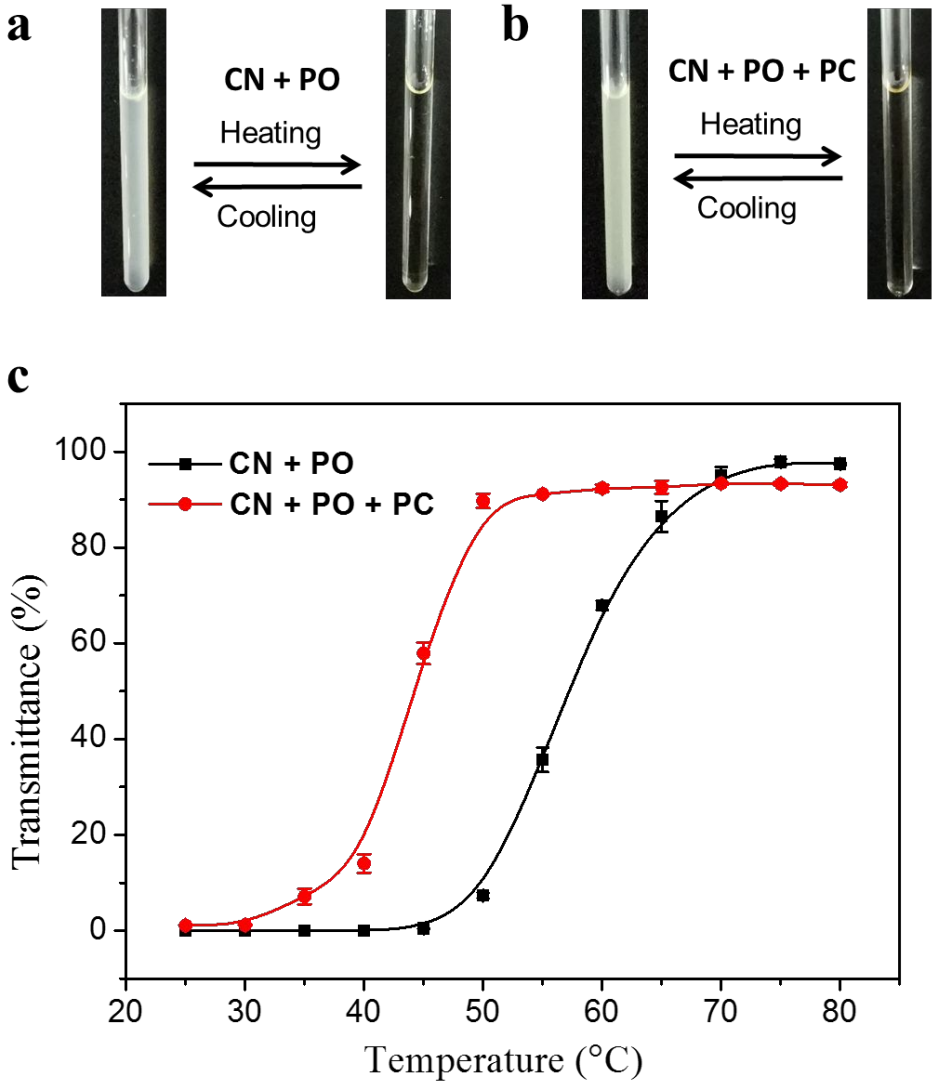

Figure S34. Photographs (a, b) and temperature dependence of the transmittance (c) of dynamic reactions in Figure S33 during a heating/cooling process.

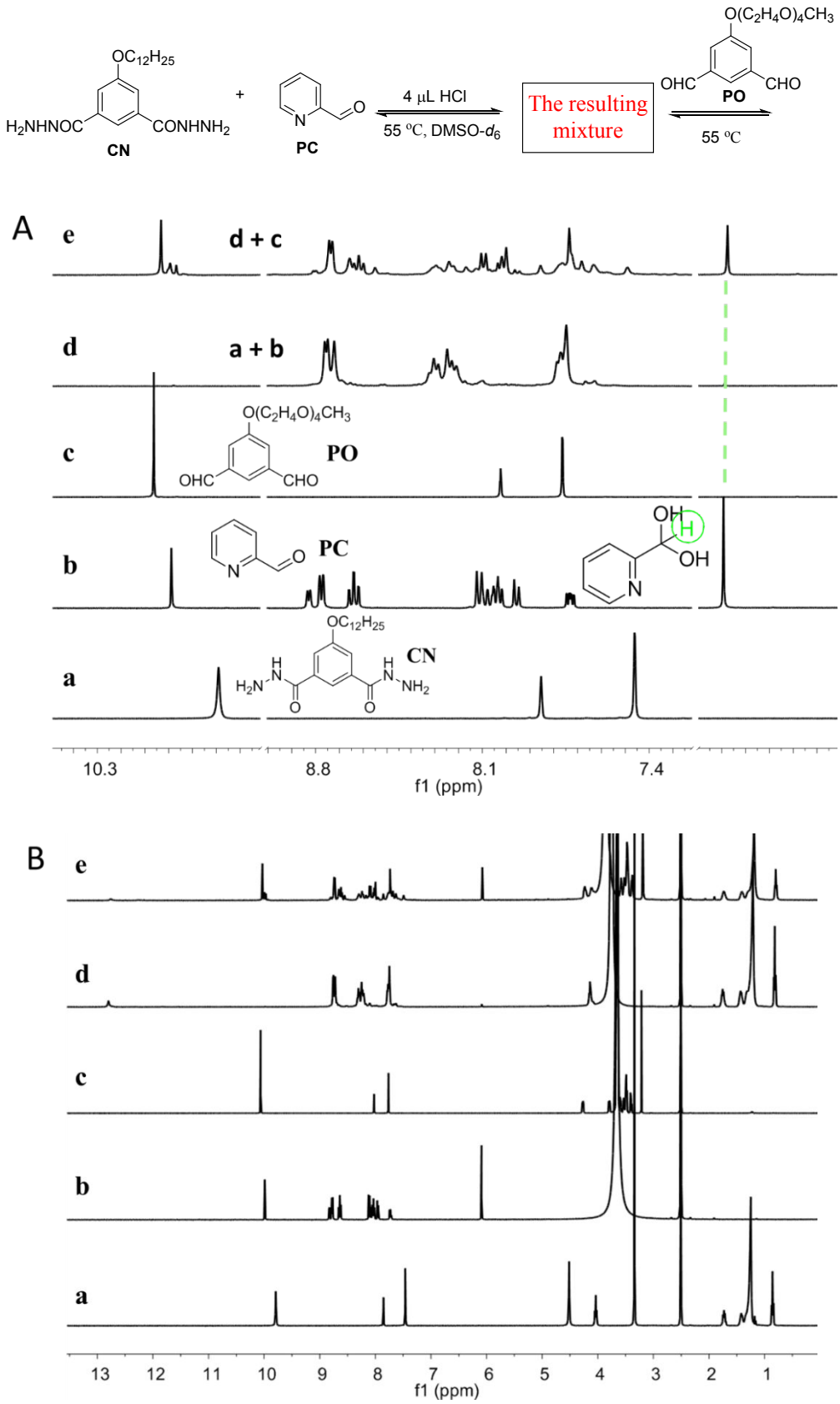

Figure S35. (A) Dynamic component exchange between **PC** and **PO** in the presence of HCl in DMSO-d_6: **CN** (a); **PC** (b); **PO** (c); the reaction of **CN** with **PC** in the presence of HCl (d); the addition of **PO** into panel d (e); (B) The full ^{1}H NMR spectra of **A**. This figure shows the NMR spectra of entry 5 in Table 1 in the main text.

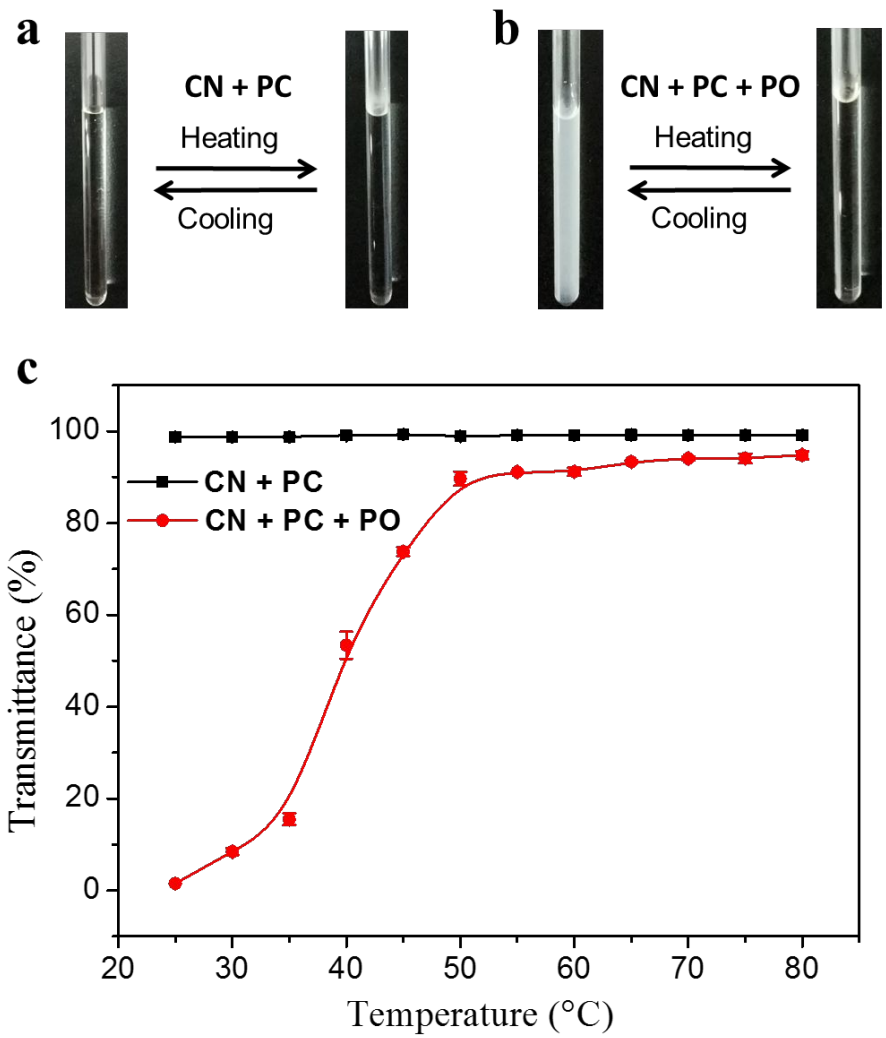

Figure S36. Photographs (a, b) and temperature dependence of the transmittance (c) of dynamic reactions in Figure S35 during a heating/cooling process.

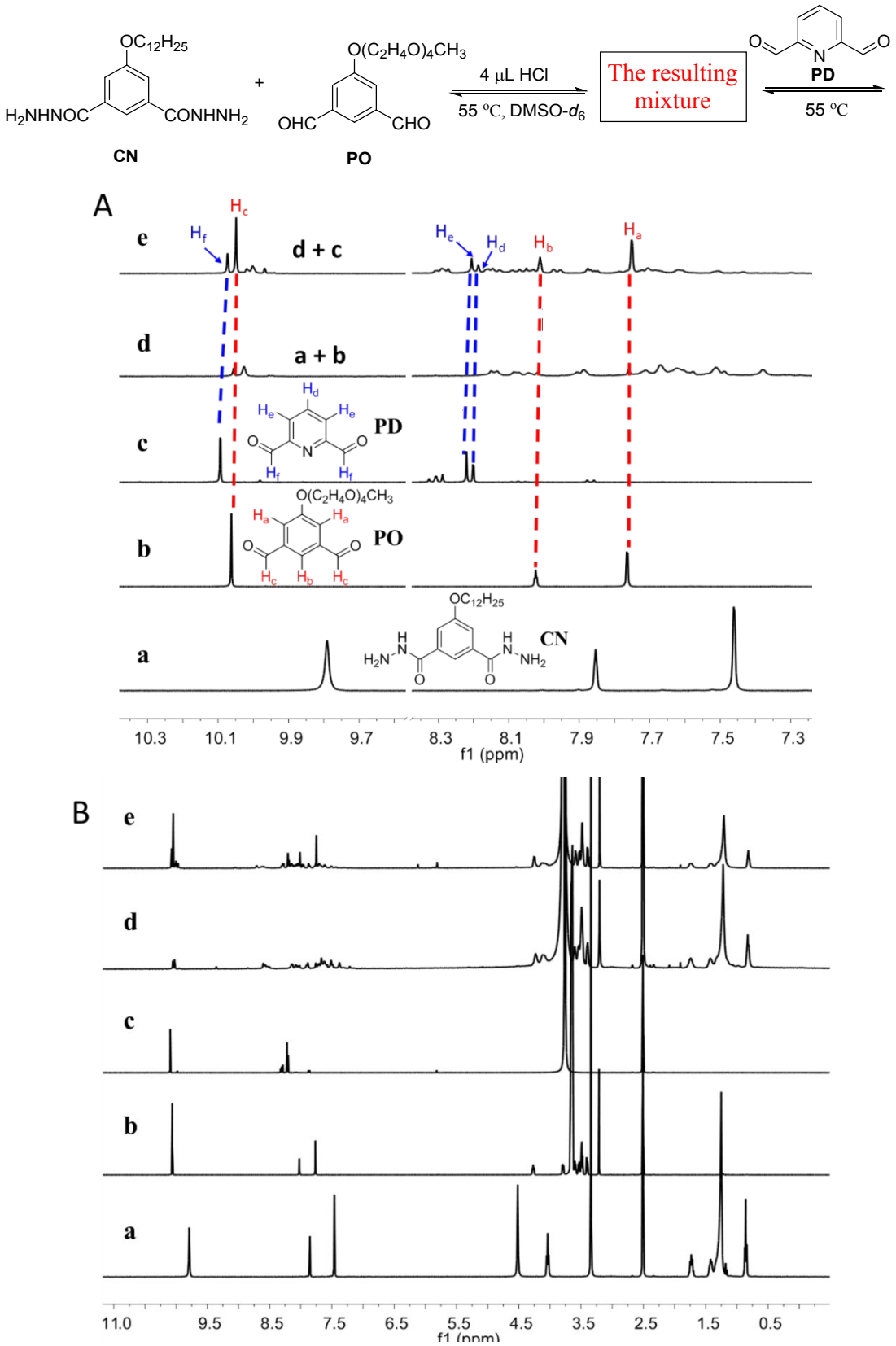

Figure S37. (A) Dynamic component exchange between **PO** and **PD** in the presence of HCl in DMSO-d_6: **CN** (a); **PO** (b); **PD** (c); the reaction of **CN** with **PO** in the presence of HCl (d); the addition of **PD** into panel d (e); (B) The full ^{1}H NMR spectra of A. This figure shows the NMR spectra of entry 6 in Table 1 in the main text.

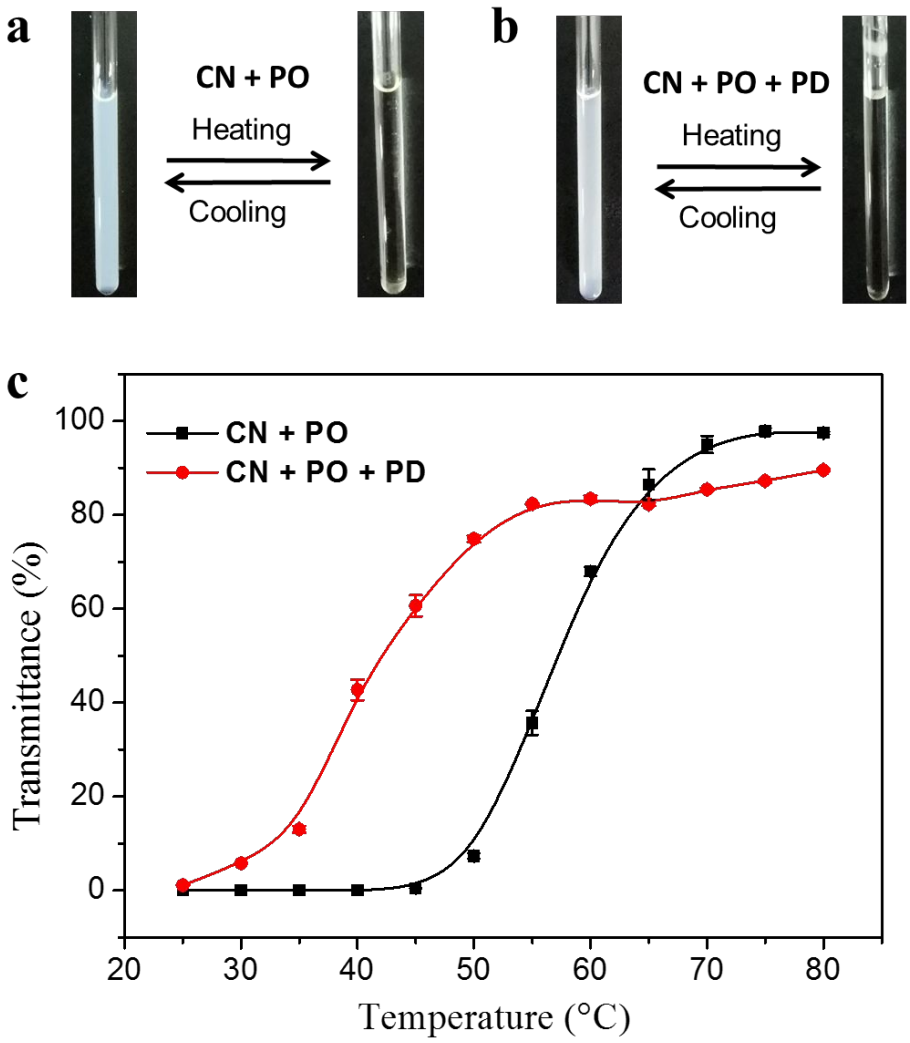

Figure S38. Photographs (a, b) and temperature dependence of the transmittance (c) of dynamic reactions in Figure S37 during a heating/cooling process.

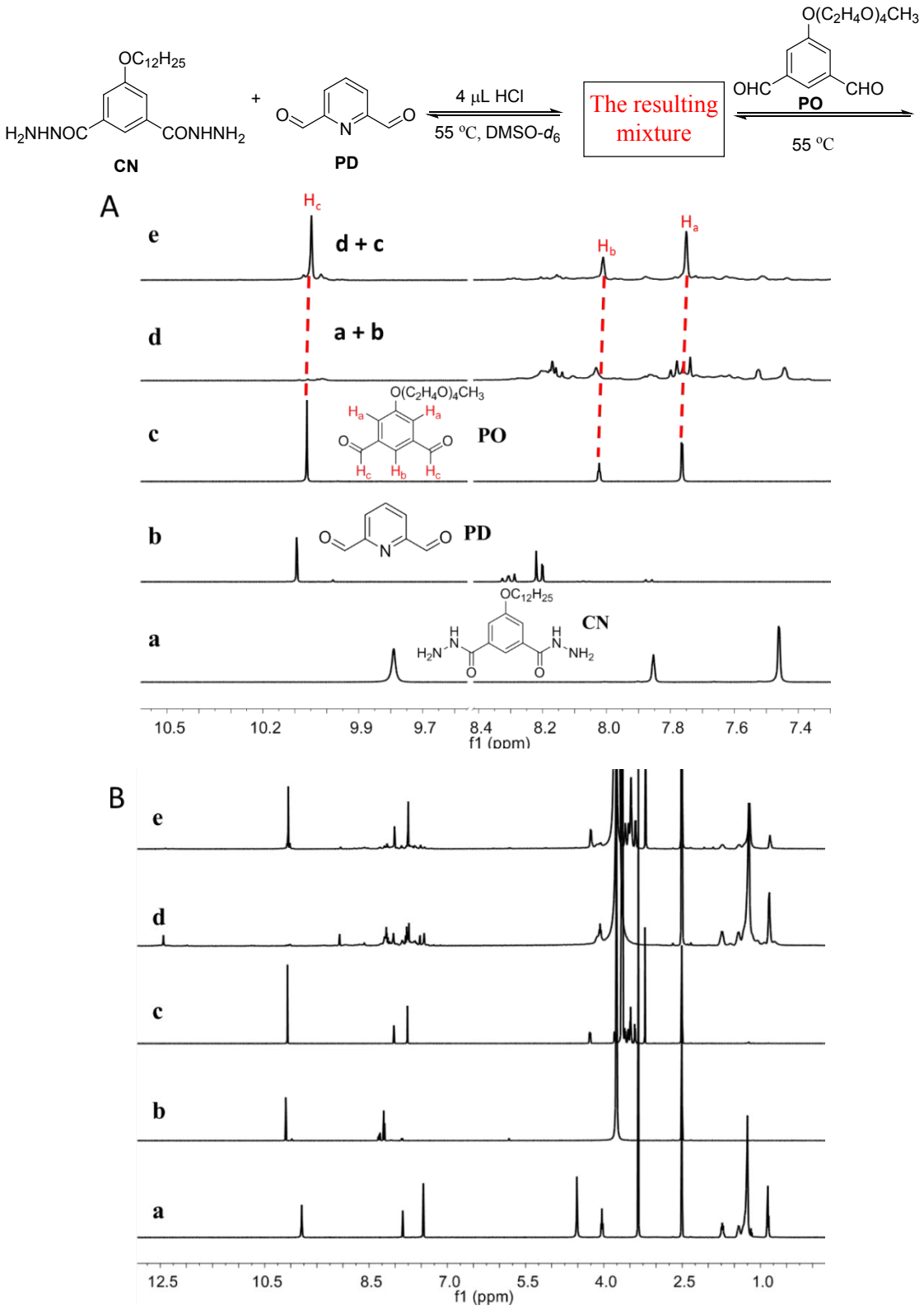

Figure S39. (A) Dynamic component exchange between **PD** and **PO** in the presence of HCl in DMSO-d_6: **CN** (a); **PD** (b); **PO** (c); the reaction of **CN** with **PD** in the presence of HCl (d); the addition of **PO** into panel d (e); (B) The full ^{1}H NMR spectra of A. This figure shows the NMR spectra of entry 7 in Table 1 in the main text.

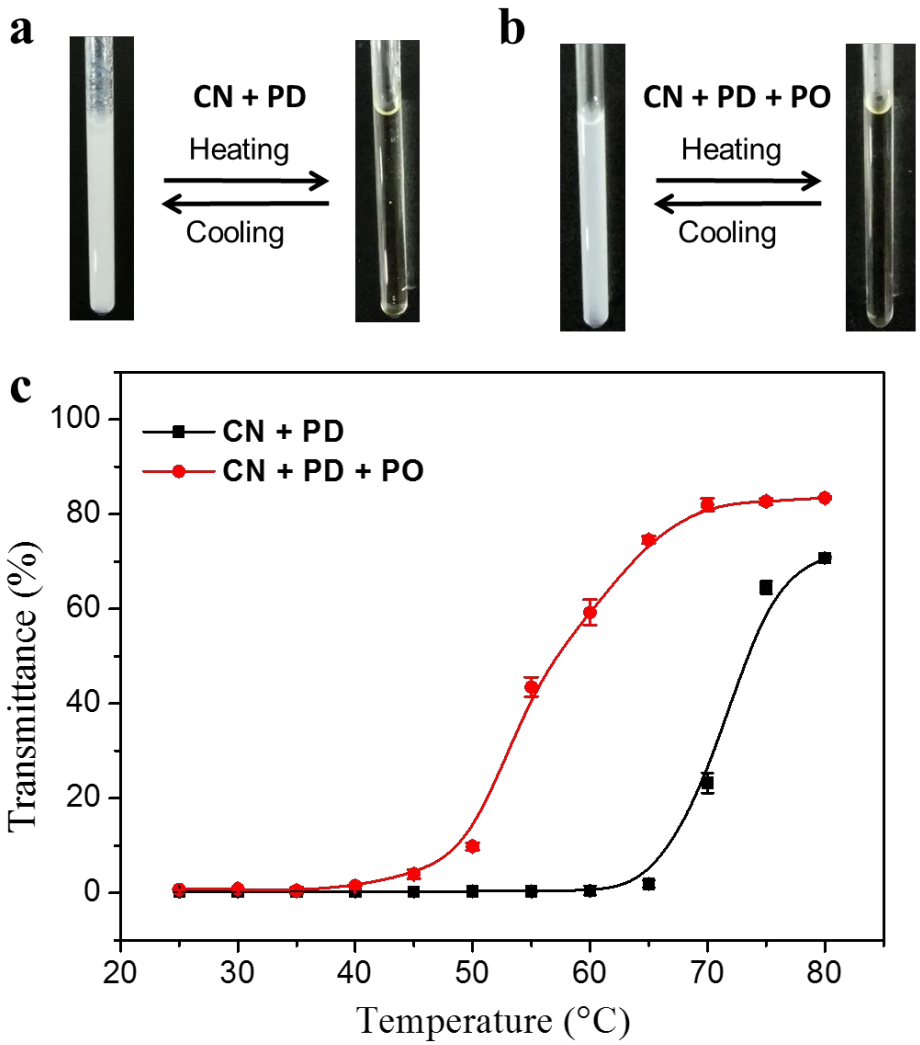

Figure S40. Photographs (a, b) and temperature dependence of the transmittance (c) of dynamic reactions in Figure S39 during a heating/cooling process.

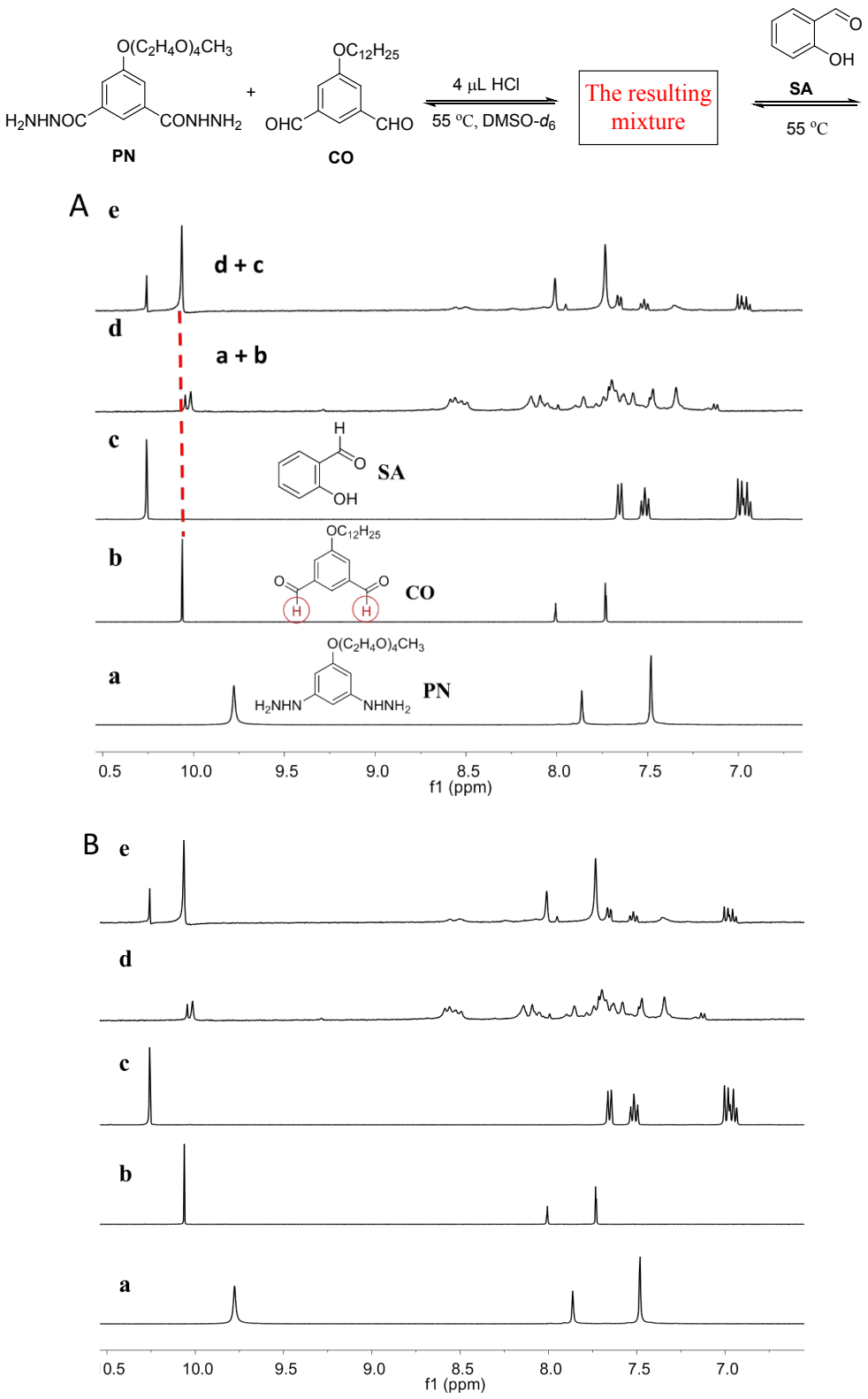

Figure S41. (A) Dynamic component exchange between **CO** and **SA** in the presence of HCl in DMSO-d_6: **PN** (a); **CO** (b); **SA** (c); the reaction of **PN** with **CO** in the presence of HCl (d); the addition of **SA** into panel d (e); (B) The full ^{1}H NMR spectra of **A**. This figure shows the NMR spectra of entry 8 in Table 1 in the main text.

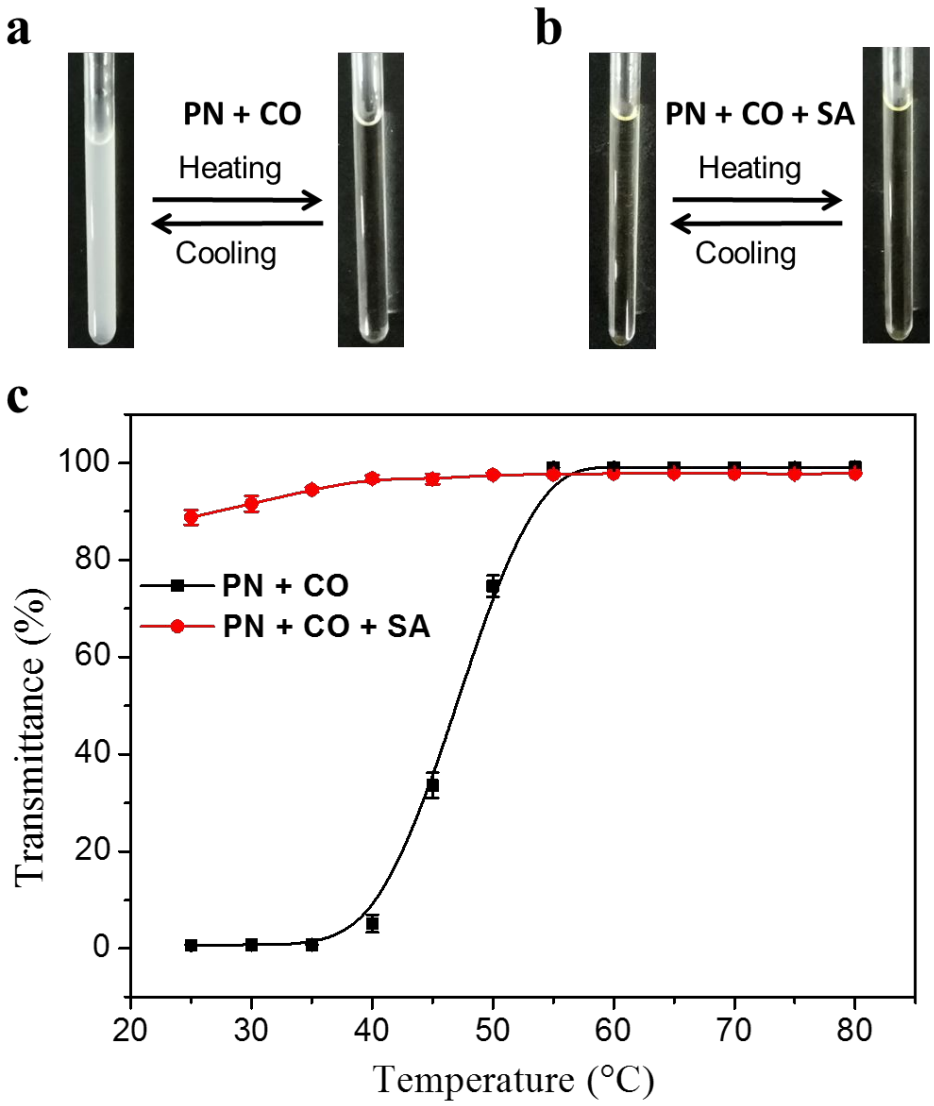

Figure S42. Photographs (a, b) and temperature dependence of the transmittance (c) of dynamic reactions in Figure S41 during a heating/cooling process.

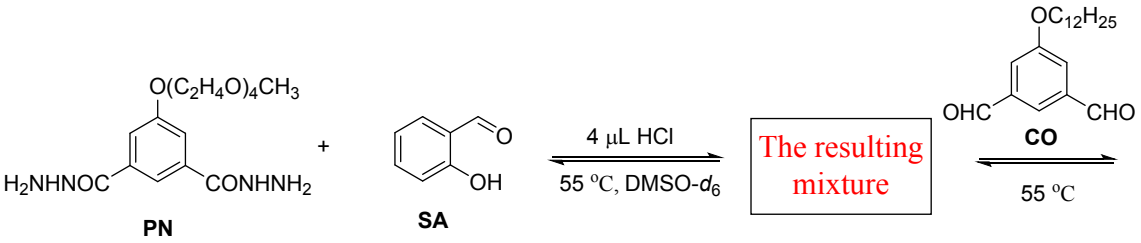

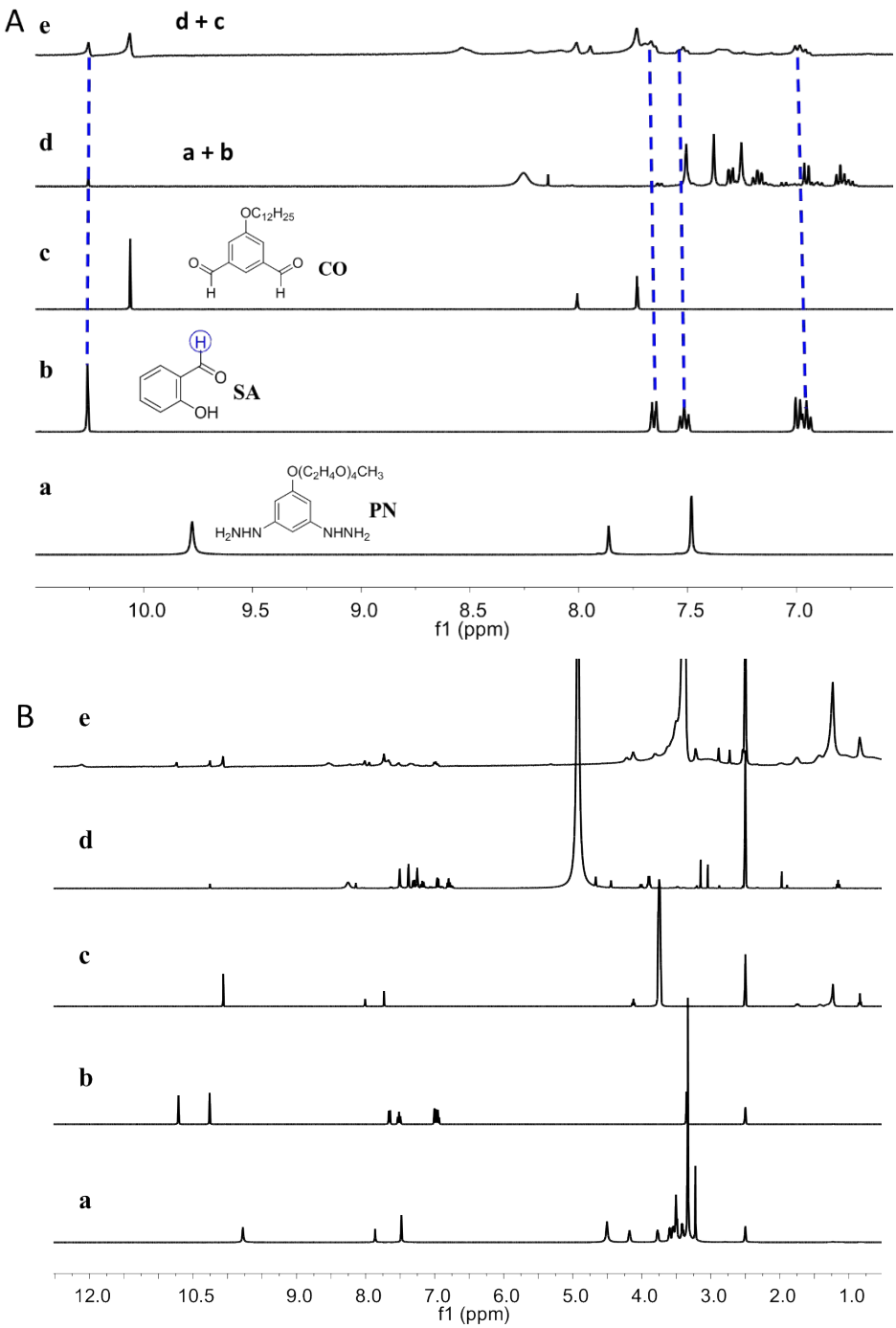

Figure S43. (A) Dynamic component exchange between **SA** and **CO** in the presence of HCl in DMSO-d_6: **PN** (a); **SA** (b); **CO** (c); the reaction of **PN** with **SA** in the presence of HCl (d); the addition of **CO** into panel d (e); (B) The full ^{1}H NMR spectra of **A**. This figure shows the NMR spectra of entry 9 in Table 1 in the main text.

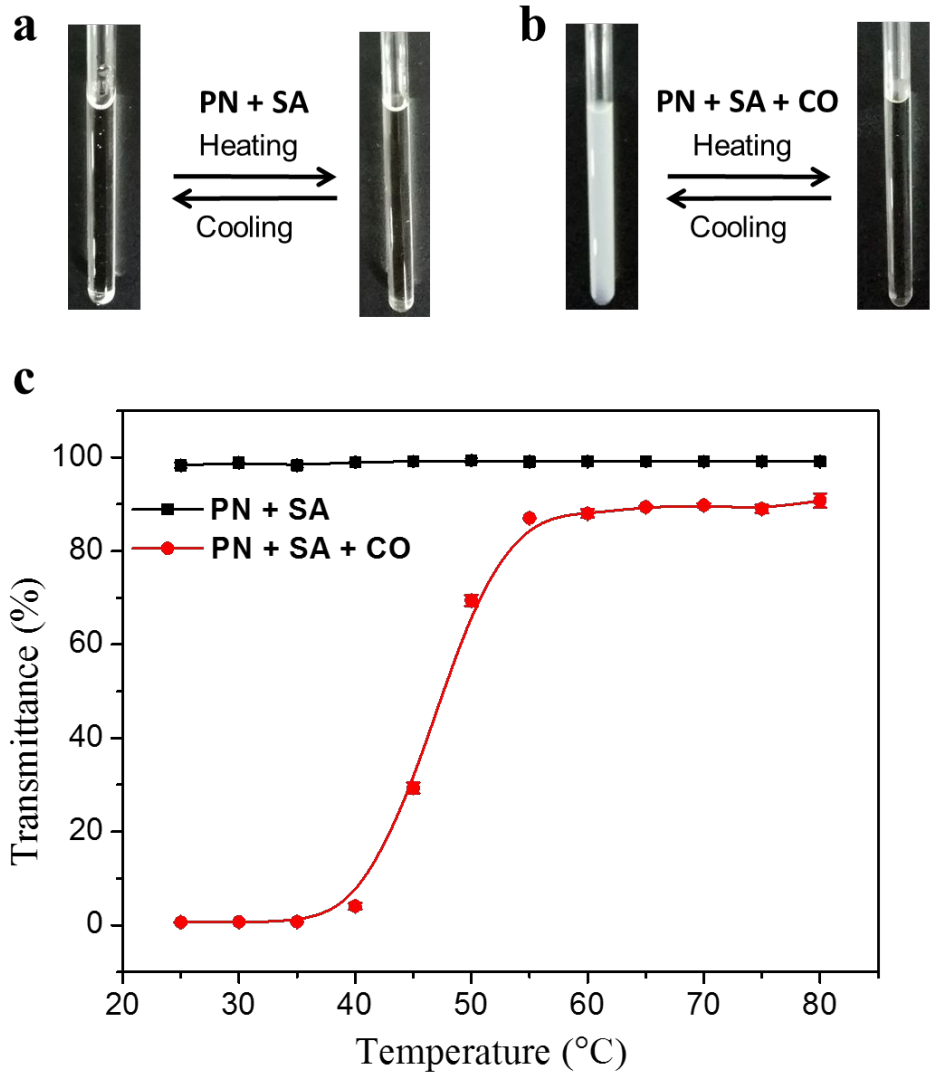

Figure S44. Photographs (a, b) and temperature dependence of the transmittance (c) of dynamic reactions in Figure S43 during a heating/cooling process.

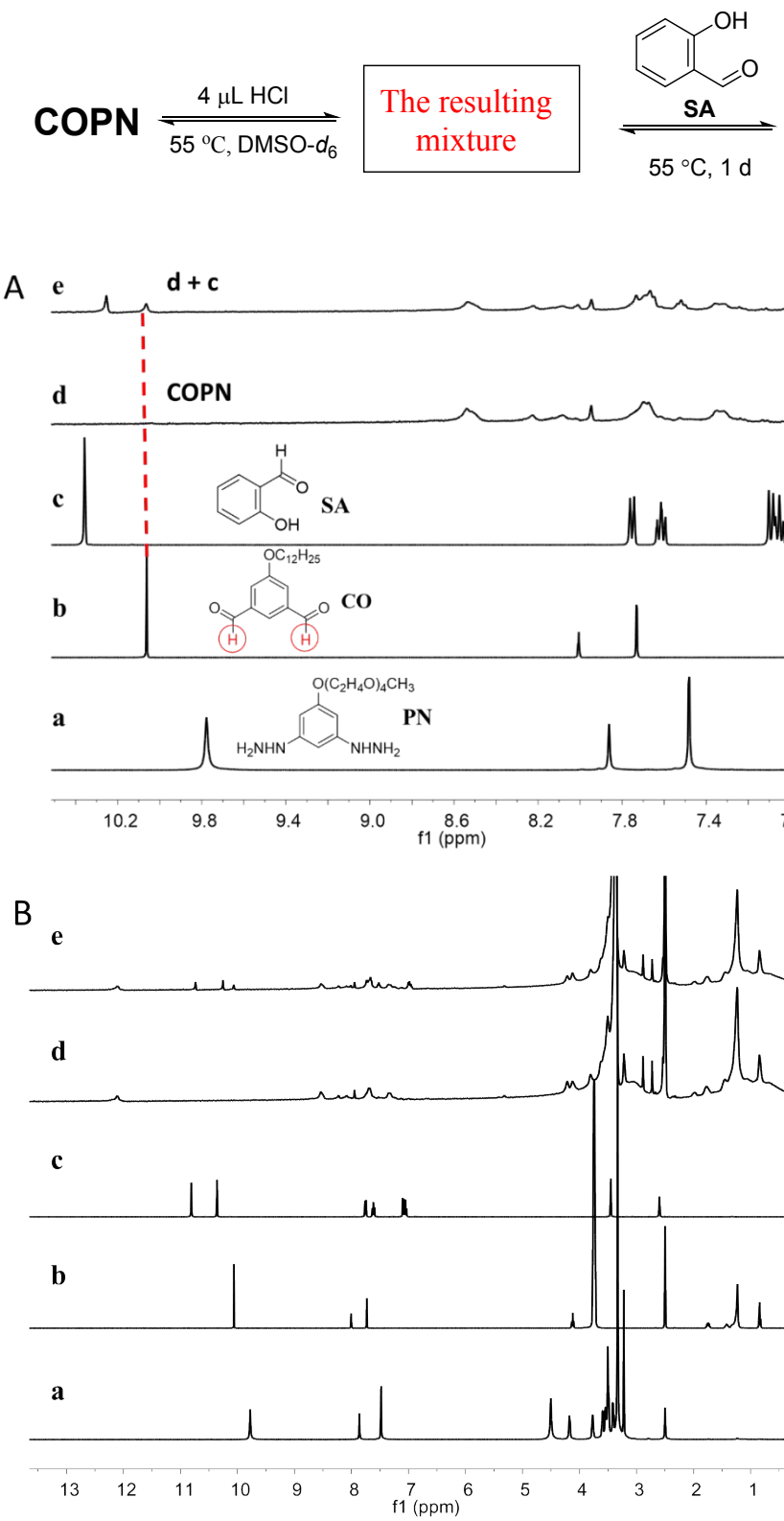

Figure S45. A) Dynamic component exchange between **CO** and **SA** in the presence of HCl in DMSO-d_6: **PN** (a); **CO** (b); **SA** (c); **COPN** (d); the addition of **SA** into panel d (e); (B) The full ^{1}H NMR spectra of A. This figure shows the NMR spectra of entry 10 in Table 1 in the main text.

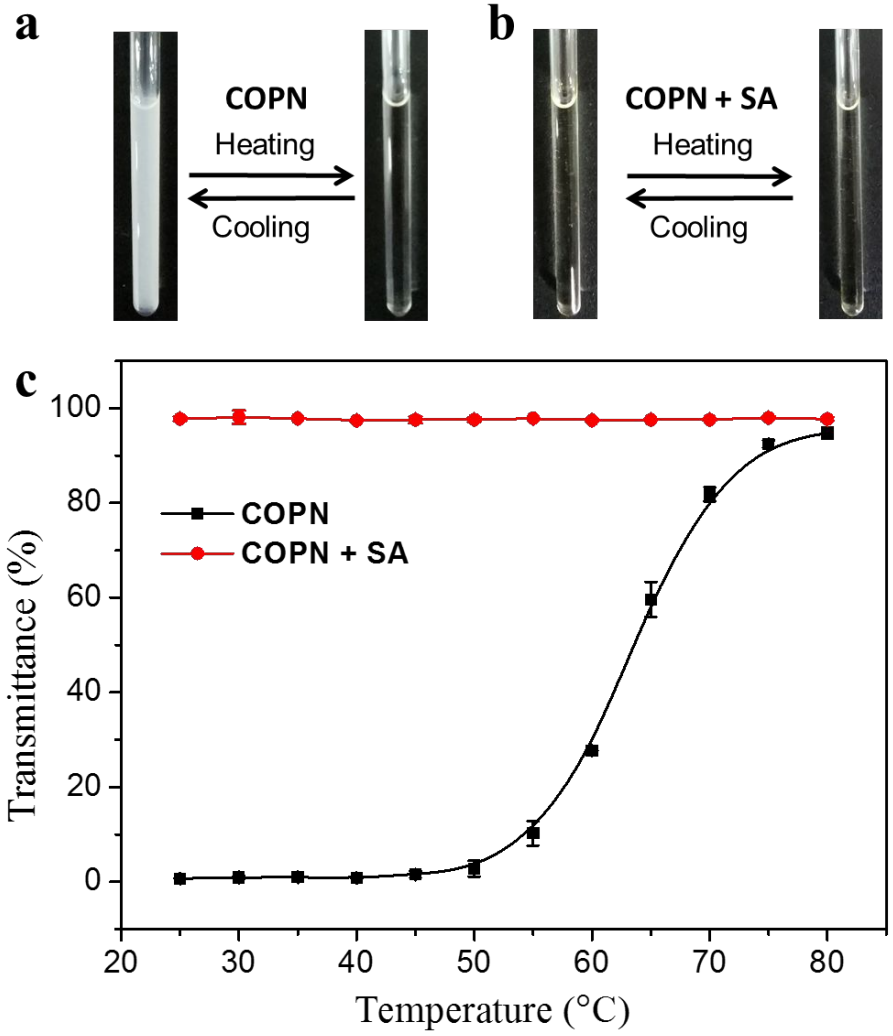

Figure S46. Photographs (a, b) and temperature dependence of the transmittance (c) of dynamic reactions in Figure S45 during a heating/cooling process.

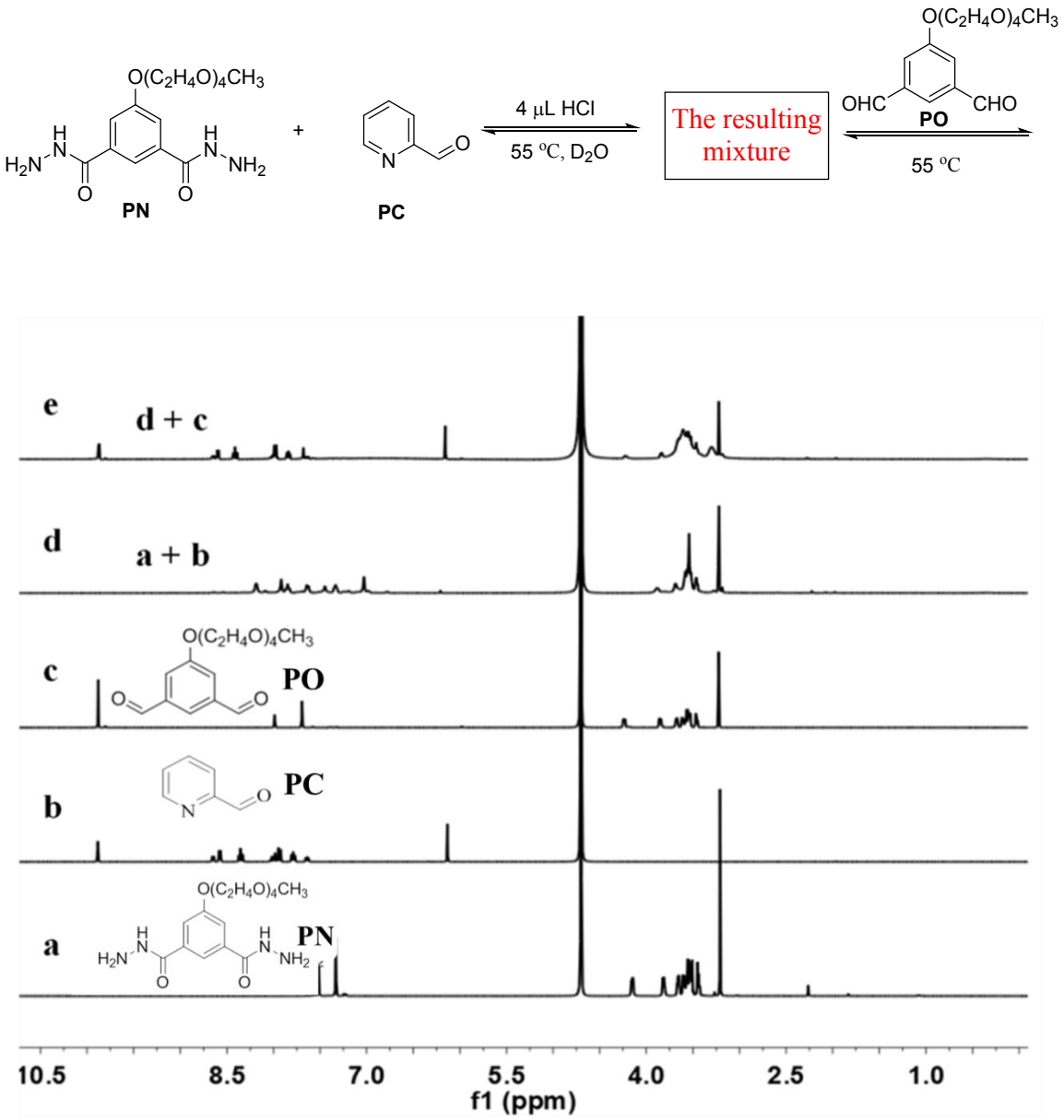

Figure S47. Dynamic component exchange between **PC** and **PO** in the presence of HCl in D_2O: **PN** (a); **PC** (b); **PO** (c); the reaction of **PN** with **PC** in the presence of HCl (d); the addition of **PO** into panel d (e). This figure shows the NMR spectra of entry 11 in Table 1 in the main text.

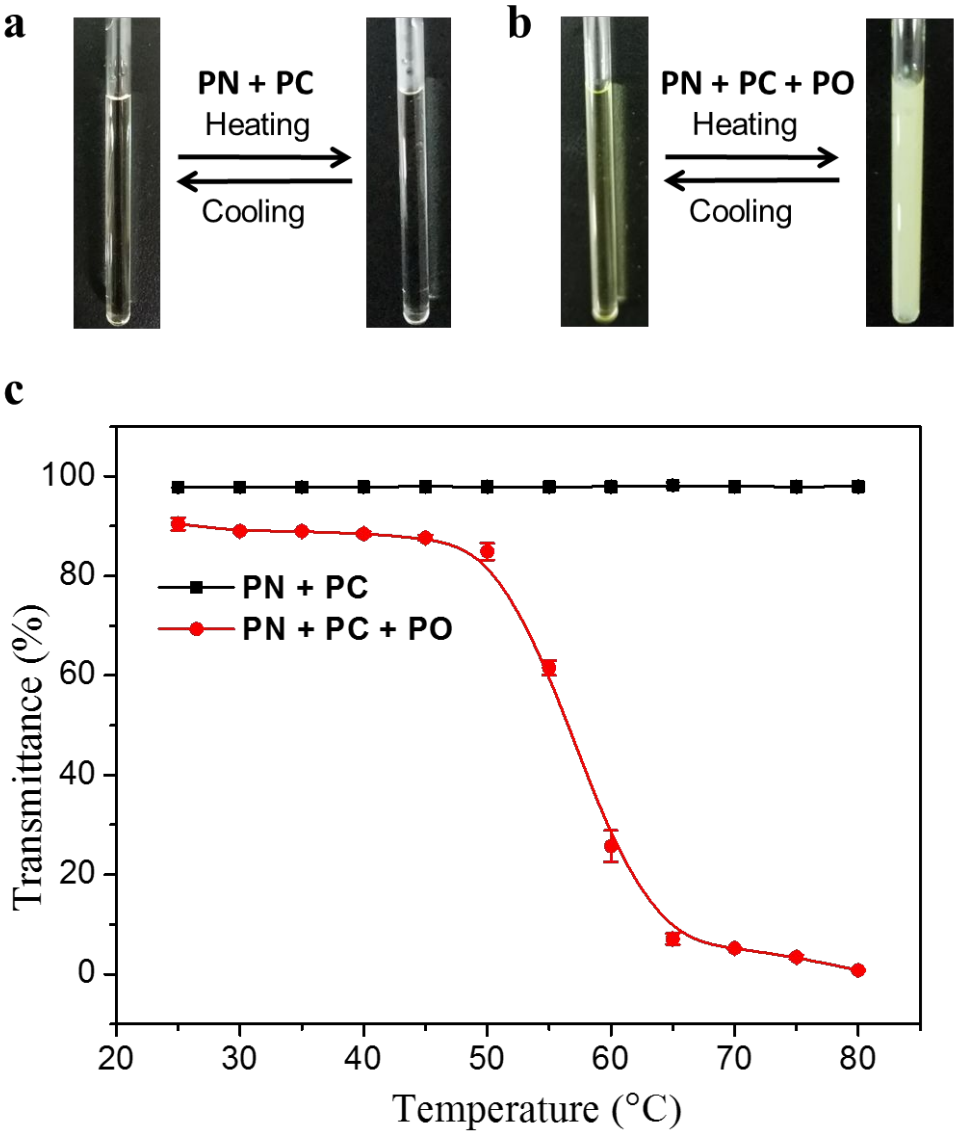

Figure S48. Photographs (a, b) and temperature dependence of the transmittance (c) of dynamic reactions in Figure S47 during a heating/cooling process.

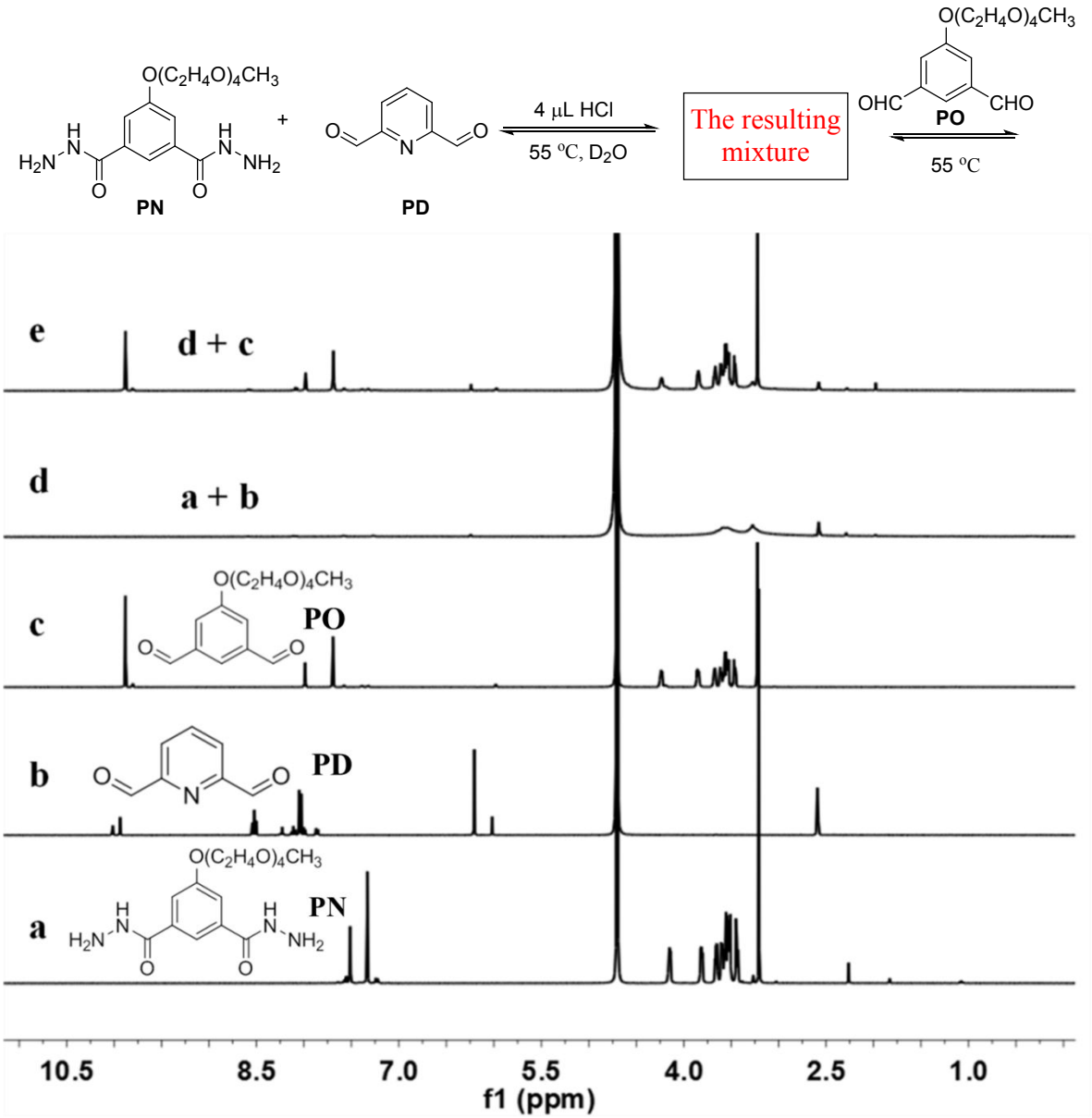

Figure S49. Dynamic component exchange between **PD** and **PO** in the presence of HCl in D_2O: **PN** (a); **PD** (b); **PO** (c); the reaction of **PN** with **PD** in the presence of HCl (d); the addition of **PO** into panel d (e). This figure shows the NMR spectra of entry 12 in Table 1 in the main text.

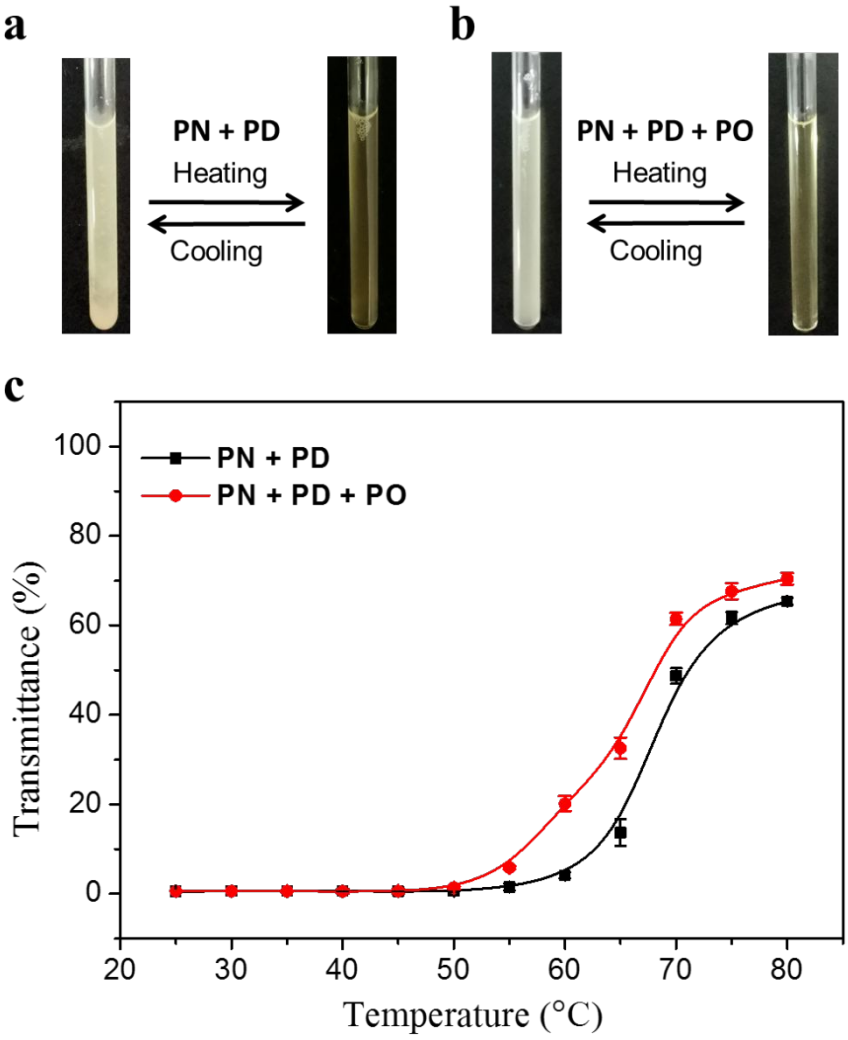

Figure S50. Photographs (a, b) and temperature dependence of the transmittance (c) of dynamic reactions in Figure S49 during a heating/cooling process.

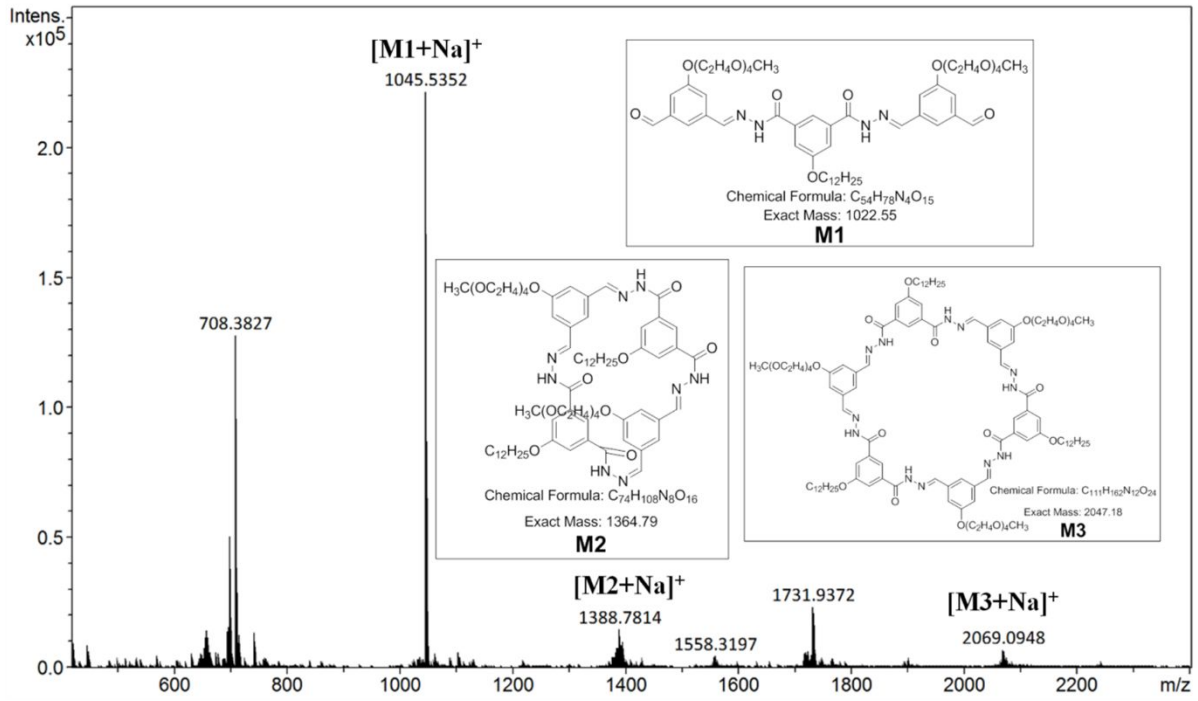

Figure S51. ESI mass spectrum of the reaction of **CN** with **PO** in the presence of HCl in DMSO.

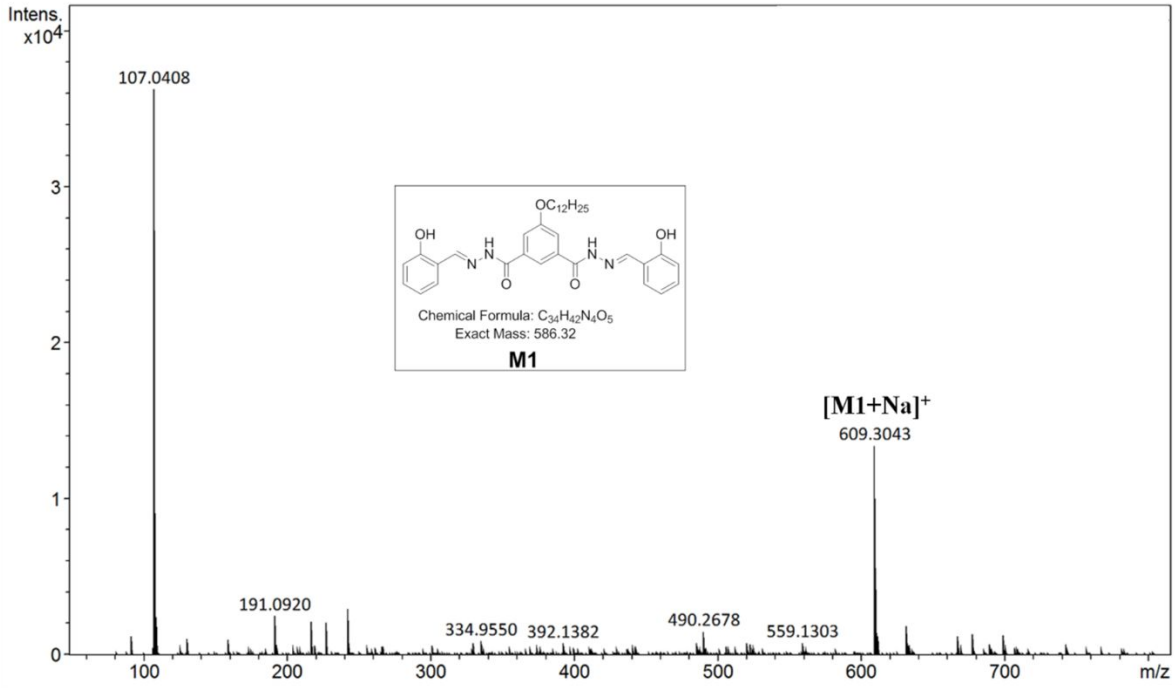

Figure S52. ESI mass spectrum of the reaction of **CN** with **SA** in the presence of HCl in DMSO.

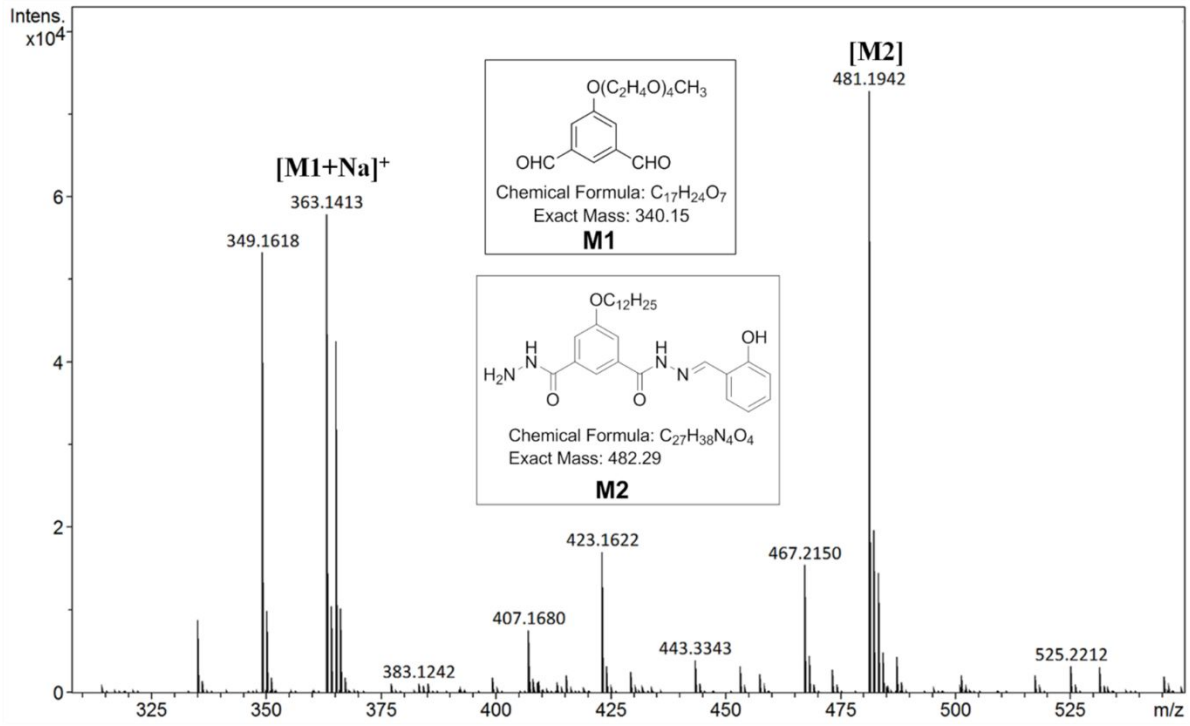

Figure S53. ESI mass spectrum of the addition of **SA** into the reaction of **CN** with **PO** in the presence of HCl in DMSO. This is the corresponding mass spectrum of Figure S26.

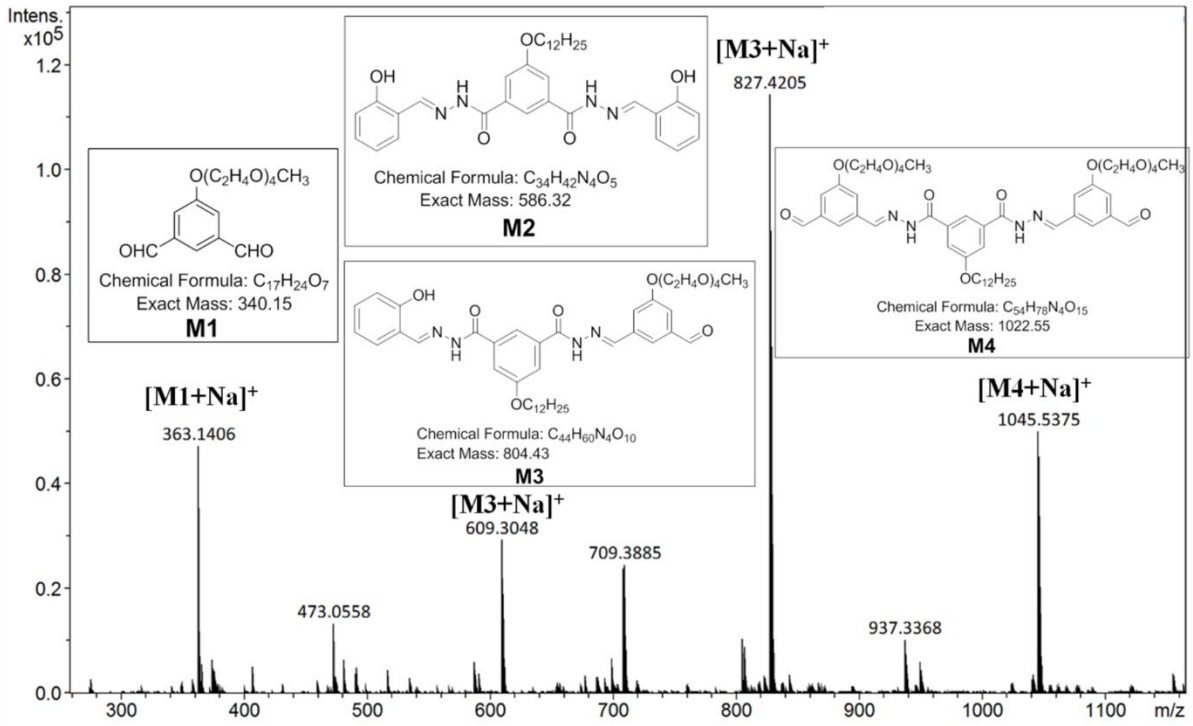

Figure S54. ESI mass spectrum of the addition of **PO** into the reaction of **CN** with **SA** in the presence of HCl in DMSO. This is the corresponding mass spectrum of Figure S29.

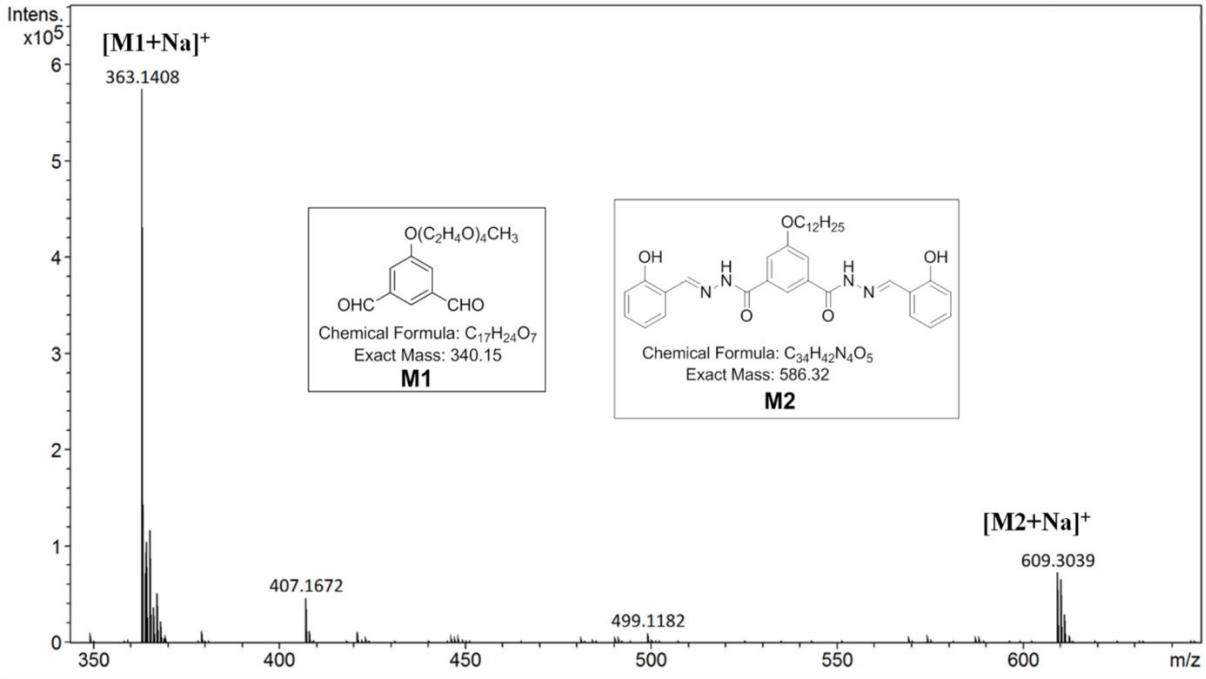

Figure S55. ESI mass spectrum of the addition of **PO** into the reaction of **CN** with **SA** in the presence of HCl and then NaOH (to increase pH) in DMSO. This is the corresponding mass spectrum of Figure S30.

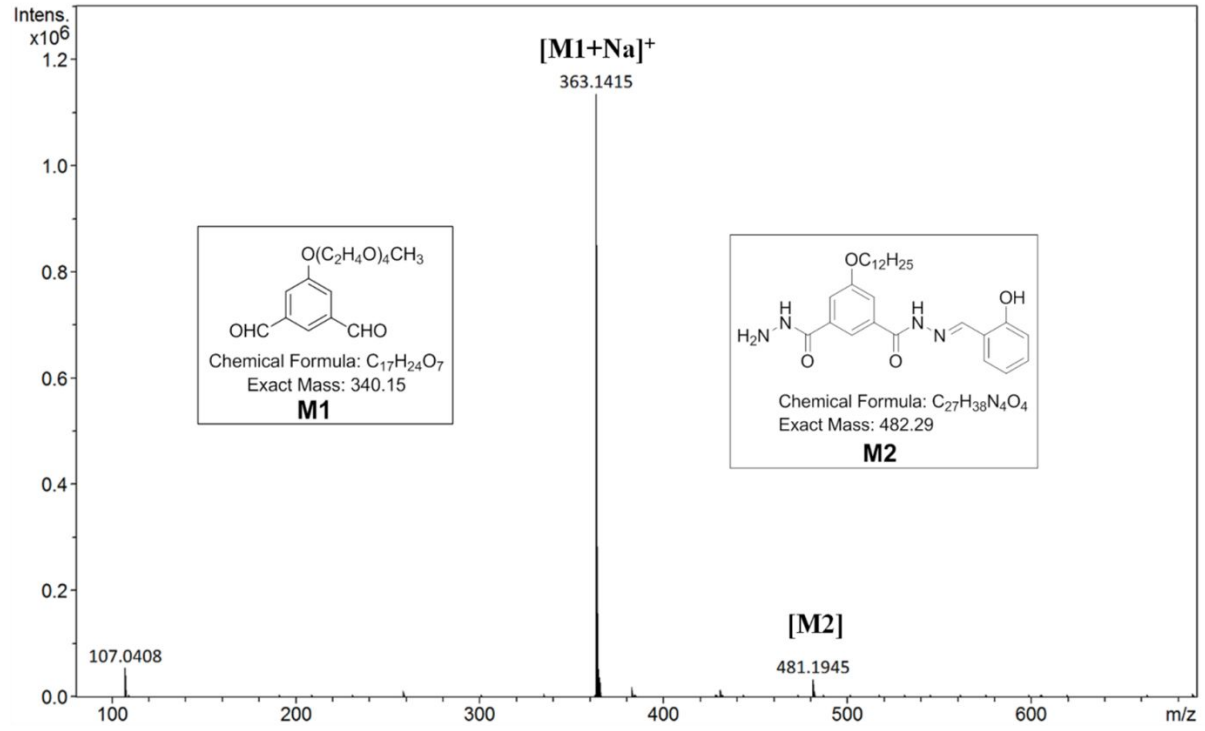

Figure S56. ESI mass spectrum of the reaction **POCN** with **SA** in the presence of HCl in DMSO. This is the corresponding mass spectrum of Figure S31.

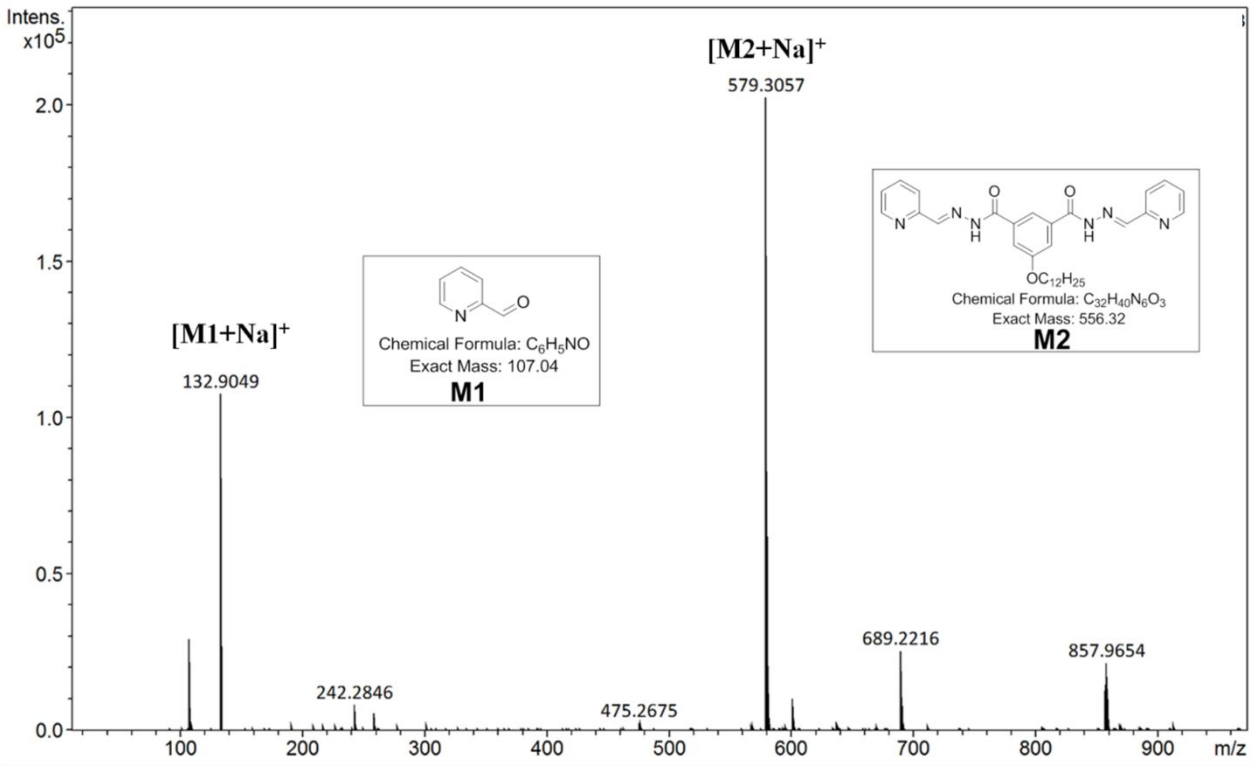

Figure S57. ESI mass spectrum of the reaction of **CN** with **PC** in the presence of HCl in DMSO.

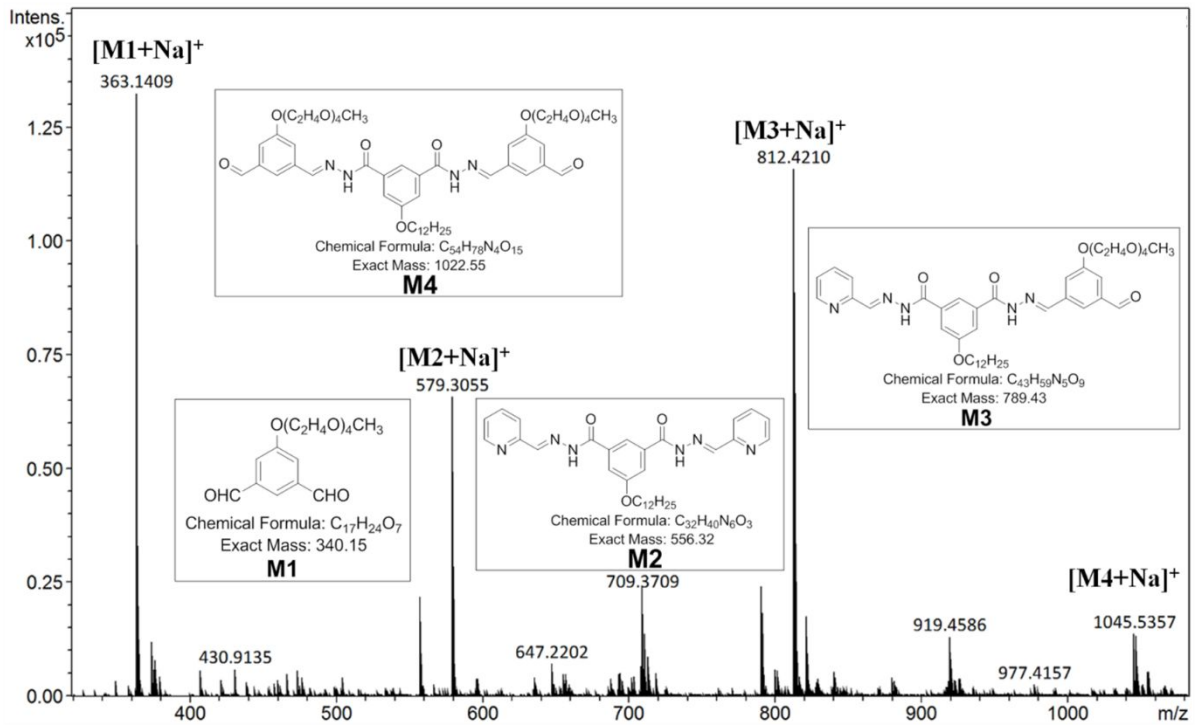

Figure S58. ESI mass spectrum of the addition of **PC** into the reaction of **CN** with **PO** in the presence of HCl in DMSO. This is the corresponding mass spectrum of Figure S33.

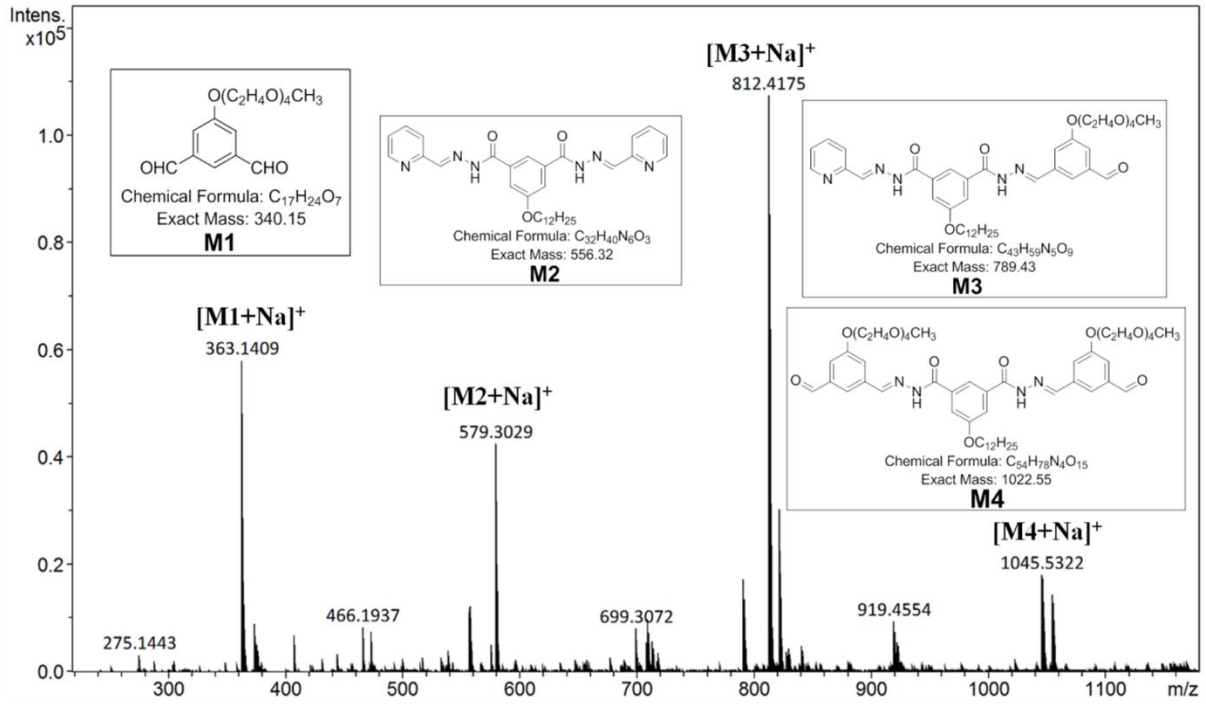

Figure S59. ESI mass spectrum of the addition of **PO** into the reaction of **CN** with **PC** in the presence of HCl in DMSO. This is the corresponding mass spectrum of Figure S35.

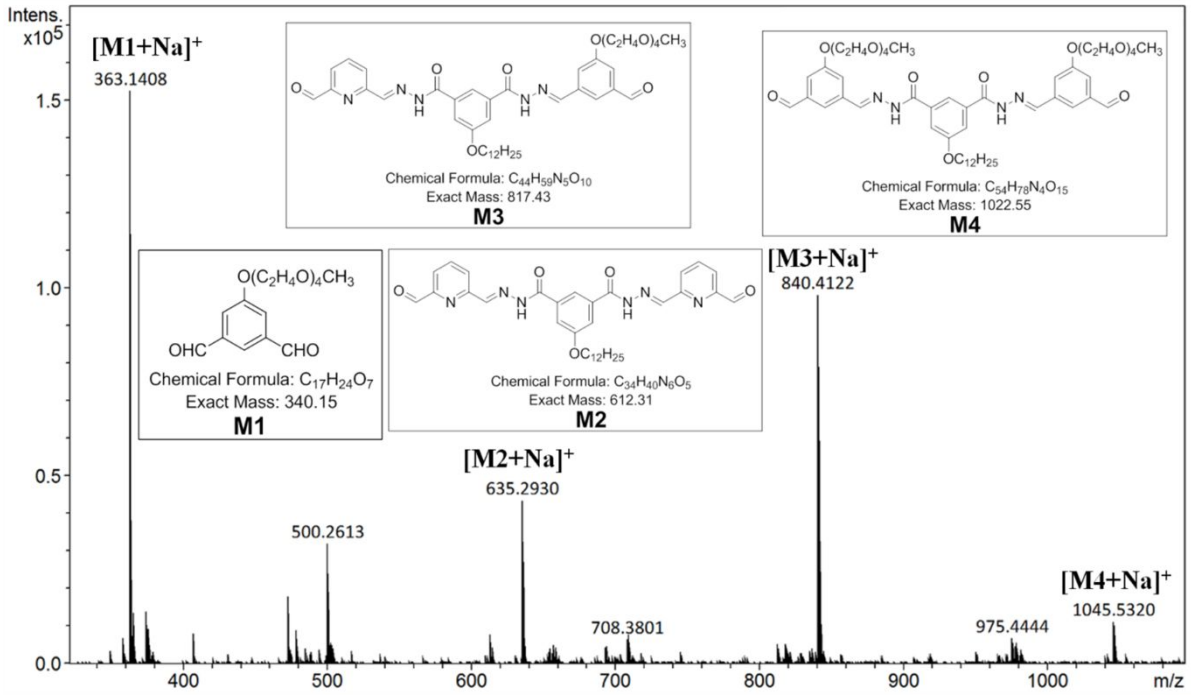

Figure S60. ESI mass spectrum of the addition of **PD** into the reaction of **CN** with **PO** in the presence of HCl in DMSO. This is the corresponding mass spectrum of Figure S37.

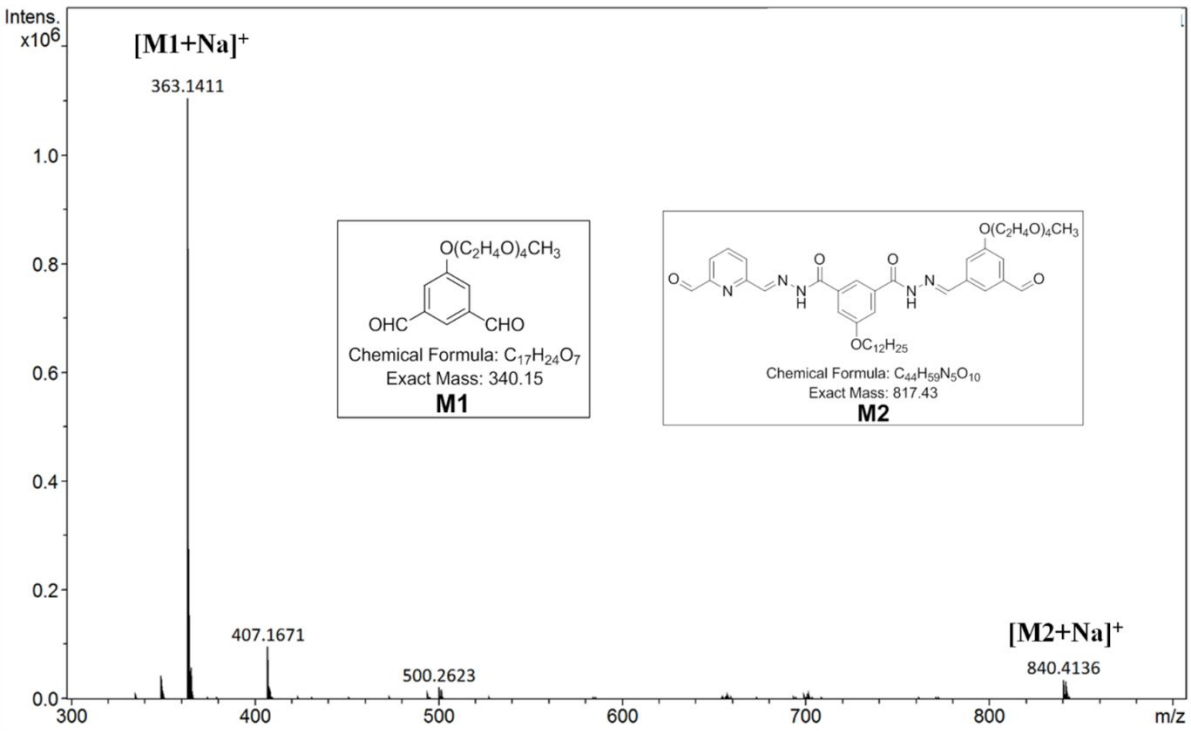

Figure S61. ESI mass spectrum of the addition of **PO** into the reaction of **CN** with **PD** in the presence of HCl in DMSO. This is the corresponding mass spectrum of Figure S39.

5. Encapsulation of Molecular Dyes

Table S1. Linear fitting results of the fluorescence intensity of different concentrations of NR with **POCN** (2 mg/mL) in DMSO during heating-cooling process.

	Slope	Intercept	R^2
NR	43.08	1.55	0.9998
NR + **POCN**，T = 25 °C	21.61	1.98	0.9987
NR + **POCN**，T = 70 °C	42.10	4.68	0.9981

Table S2. Linear fitting results of the fluorescence intensity of different concentrations of FS with **POPN** (2 mg/mL) in water during heating-cooling process.

	Slope	Intercept	R^2
FS	66.97	25.89	0.9986
FS + **POPN**，T = 25 °C	68.81	16.63	0.9957
FS + **POPN**，T = 70 °C	25.90	2.83	0.9991

6. DFT Calculations

Gaussian 09 package[S4] was used for geometry optimization and the calculation of energies. The DFT method and basis set of M062X-D3/Def2-SVP were employed. All geometries were found to have zero imaginary frequencies. Interaction energy ($E_{int,\ AB}$) is interpreted as the difference between the energy of the complex and the sum of the energies of its segments. It can be defined in the following equation:

$$E_{int,\ AB} = E_{AB} - E_A - E_B + BSSE$$

BSSE is the basis set superposition error correction, which is often settled down by counterpoise correction method of Boys and Bernardi.[S5]

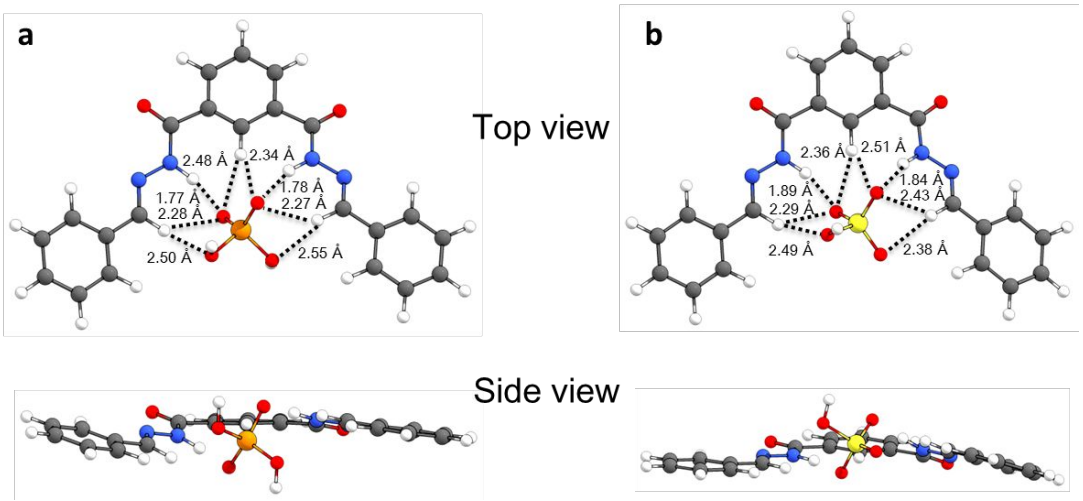

Figure S62. The optimized structures of the model complex with $H_2PO_4^-$ (a) and HSO_4^- (b) by DFT calculation, with the distance of potential hydrogen bonding listed. The simplified model was used to mimic the binding pocket of **POCN** (Scheme 2). The difference in interaction energy is -8.3 kcal/mol, favoring $H_2PO_4^-$ over HSO_4^-.

Complex with $H_2PO_4^-$
Imaginary frequency: 0
G = -1860.095729 hartree
$E_{int,\ AB}$ = -55.37 kcal/mol

C	1.20400000	4.64050000	0.08280000
C	1.20260000	3.24490000	-0.00710000
C	-0.01550000	2.55670000	-0.05750000
C	-1.22070000	3.26750000	-0.02430000
C	-1.20420000	4.66370000	0.03910000

C	0.00580000	5.34840000	0.09900000
H	2.17030000	5.14270000	0.14120000
H	-0.03430000	1.46950000	-0.13810000
H	-2.16210000	5.18560000	0.03370000
H	0.01560000	6.43820000	0.15860000
C	2.56270000	2.58430000	0.00950000
O	3.55770000	3.22290000	0.27710000
C	-2.58050000	2.61840000	-0.11720000
O	-3.55090000	3.25110000	-0.47350000
N	2.57820000	1.24470000	-0.28330000
N	-2.61640000	1.29320000	0.23350000
H	1.74000000	0.71290000	-0.58810000
H	-1.80790000	0.79920000	0.66350000
N	3.74120000	0.57280000	-0.16830000
N	-3.75330000	0.59740000	0.03520000
C	3.71230000	-0.68560000	-0.39070000
H	2.78240000	-1.20310000	-0.66400000
C	-3.74510000	-0.63570000	0.37250000
H	-2.85730000	-1.10790000	0.81520000
C	4.93690000	-1.48960000	-0.25560000
C	6.19150000	-0.89590000	-0.04780000
C	4.84590000	-2.88510000	-0.32480000
C	7.32720000	-1.68760000	0.07950000
H	6.24150000	0.19270000	0.01030000
C	5.98650000	-3.67630000	-0.19510000
H	3.86350000	-3.34240000	-0.46510000
C	7.23070000	-3.08040000	0.00450000
H	8.30000000	-1.21750000	0.23740000
H	5.90240000	-4.76340000	-0.24770000
H	8.12560000	-3.69810000	0.10230000
C	-4.92930000	-1.47770000	0.14510000
C	-4.82460000	-2.86050000	0.34070000
C	-6.15310000	-0.93610000	-0.27670000
C	-5.92460000	-3.68980000	0.12600000
H	-3.86090000	-3.27590000	0.64540000
C	-7.24820000	-1.76600000	-0.48830000
H	-6.21170000	0.14260000	-0.43140000
C	-7.13980000	-3.14530000	-0.28630000
H	-5.83110000	-4.76670000	0.27840000
H	-8.19800000	-1.33770000	-0.81510000
H	-8.00220000	-3.79350000	-0.45410000
P	-0.02810000	-1.28800000	0.20750000
O	-0.71360000	-0.46620000	1.26780000

O	-1.07530000	-2.40240000	-0.37640000
O	0.61040000	-0.61780000	-0.98310000
O	1.08330000	-2.22140000	0.95760000
H	1.02100000	-2.05340000	1.90570000
H	-1.03740000	-2.36570000	-1.33990000

Complex with HSO_4^-
Imaginary frequency: 0
G = -1916.161988 hartree
$E_{int, AB}$ = -47.04 kcal/mol

C	1.17800000	4.60560000	0.17900000
C	1.17160000	3.21740000	0.00640000
C	-0.04920000	2.54620000	-0.13730000
C	-1.24930000	3.26670000	-0.10320000
C	-1.22570000	4.65570000	0.04730000
C	-0.01410000	5.32340000	0.19490000
H	2.14580000	5.09460000	0.29430000
H	-0.07980000	1.46670000	-0.29620000
H	-2.17900000	5.18620000	0.03860000
H	0.00230000	6.40730000	0.32110000
C	2.53390000	2.55890000	0.00510000
O	3.53940000	3.21230000	0.17700000
C	-2.61090000	2.63580000	-0.27210000
O	-3.56060000	3.27960000	-0.65950000
N	2.54470000	1.20220000	-0.19450000
N	-2.66200000	1.30870000	0.06340000
H	1.68980000	0.65250000	-0.35560000
H	-1.87030000	0.84760000	0.53680000
N	3.72330000	0.54920000	-0.17690000
N	-3.79570000	0.60480000	-0.13470000
C	3.69380000	-0.71580000	-0.35110000
H	2.75030000	-1.25680000	-0.50670000
C	-3.75850000	-0.63280000	0.18050000
H	-2.85480000	-1.10640000	0.58880000
C	4.94040000	-1.49670000	-0.32790000
C	6.19450000	-0.87920000	-0.20240000
C	4.87400000	-2.89150000	-0.42770000
C	7.35290000	-1.64750000	-0.18210000
H	6.22600000	0.20860000	-0.12200000
C	6.03760000	-3.65930000	-0.40620000
H	3.89560000	-3.36970000	-0.51500000
C	7.28020000	-3.04000000	-0.28510000
H	8.32480000	-1.15940000	-0.08470000

H	5.97260000	-4.74620000	-0.48350000
H	8.19250000	-3.63950000	-0.27010000
C	-4.92730000	-1.50200000	-0.01590000
C	-4.78070000	-2.87840000	0.19810000
C	-6.17180000	-0.99510000	-0.41750000
C	-5.86430000	-3.73680000	0.01860000
H	-3.79940000	-3.26170000	0.49010000
C	-7.24990000	-1.85510000	-0.59430000
H	-6.26220000	0.07960000	-0.58470000
C	-7.10120000	-3.22800000	-0.37510000
H	-5.74070000	-4.80870000	0.18380000
H	-8.21710000	-1.45610000	-0.90650000
H	-7.95000000	-3.90020000	-0.51460000
S	-0.10620000	-1.34040000	0.50000000
O	0.50970000	-0.78140000	-0.71560000
O	-0.69920000	-0.30670000	1.37850000
O	-0.95240000	-2.50480000	0.28840000
O	1.19820000	-1.85190000	1.35640000
H	0.97480000	-1.73230000	2.28980000

7. References

S1. Zha, D. J.; You, L. Multiresponsive Dynamic Covalent Assemblies for the Selective Sensing of Both Cu^{2+} and CN^{-} in Water. *ACS Appl. Mater. Interfaces.* **2016**, *8*, 2399−2405.

S2. Bodio, E.; Boujtita, M.; Julienne, K.; Le Saec, P.; Gouin, S. G.; Hamon, J.; Renault, E.; Deniaud, D. Synthesis and Characterization of a Stable Copper(I) Complex for Radiopharmaceutical Applications. *Chempluschem* **2014**, *79*, 1284−1293.

S3. Folmer-Andersen, J. F.; Buhler, E.; Candau, S.-J.; Joulie, S.; Schmutz, M.; Lehn, J.-M. Cooperative, Bottom-up Generation of Rigid-Rod Nanostructures through Dynamic Polymer Chemistry. *Polym. Int.* **2010**, *59*, 1477−1491.

S4. Frisch, M. J.; Trucks, G. W.; Schlegel, H. B.; Scuseria, G. E.; Robb, M. A.; Cheeseman, J. R.; Scalmani, G.; Barone, V.; Mennucci, B.; Petersson, G. A.; Nakatsuji, H.; Caricato, M.; Li, X.; Hratchian, H. P.; Izmaylov, A. F.; Bloino, J.; Zheng, G.; Sonnenberg, J. L.; Hada, M.; Ehara, M.; Toyota, K.; Fukuda, R.; Hasegawa, J.; Ishida, M.; Nakajima, T.; Honda, Y.; Kitao, O.; Nakai, H.; Vreven, T.; Montgomery, J. A., Jr.; Peralta, J. E.; Ogliaro, F.; Bearpark, M.; Heyd, J. J.; Brothers, E.; Kudin, K. N.; Staroverov, V. N.; Kobayashi, R.; Normand, J.; Raghavachari, K.; Rendell, A.; Burant, J. C.; Iyengar, S. S.; Tomasi, J.; Cossi, M.; Rega, N.; Millam, J. M.; Klene, M.; Knox, J. E.; Cross, J. B.; Bakken, V.; Adamo, C.; Jaramillo, J.; Gomperts, R.; Stratmann, R. E.; Yazyev, O.; Austin, A. J.; Cammi, R.; Pomelli, C.; Ochterski, J. W.; Martin, R. L.; Morokuma, K.; Zakrzewski, V. G.; Voth, G. A.; Salvador, P.; Dannenberg, J. J.; Dapprich, S.; Daniels, A. D.; Farkas, Ö.; Foresman, J. B.; Ortiz, J. V.; Cioslowski, J.; Fox, D. J. *Gaussian 09*, revision E.01; Gaussian, Inc.:
Wallingford, CT, **2010**.

S5. Boys, S. F.; Bernardi, F. The Calculation of Small Molecular Interactions by The Differences of Separate Total Energies. Some Procedures with Reduced Errors. *Mol. Phys.* **1970**, *19*, 553-566.